

## RESEARCH ARTICLE

# Characterization of covalent inhibitors that disrupt the interaction between the tandem SH2 domains of SYK and FCER1G phospho-ITAM

Frances M. Bashore<sup>1</sup>, Vittorio L. Katis<sup>2</sup>, Yuhong Du<sup>3,4</sup>, Arunima Sikdar<sup>5</sup>, Dongxue Wang<sup>3,4</sup>, William J. Bradshaw<sup>2</sup>, Karolina A. Rygiel<sup>2</sup>, Tina M. Leisner<sup>5</sup>, Rod Chalk<sup>2</sup>, Swati Mishra<sup>6,7</sup>, C. Andrew Williams<sup>6,7</sup>, Opher Gileadi<sup>2\*</sup>, Paul E. Brennan<sup>2</sup>, Jesse C. Wiley<sup>8</sup>, Jake Gockley<sup>8</sup>, Gregory A. Cary<sup>9</sup>, Gregory W. Carter<sup>9</sup>, Jessica E. Young<sup>6,7</sup>, Kenneth H. Pearce<sup>5</sup>, Haian Fu<sup>3,4</sup>, the Emory-Sage-SGC TREAT-AD Center<sup>†</sup>, Alison D. Axtman<sup>1\*</sup>



## OPEN ACCESS

**Citation:** Bashore FM, Katis VL, Du Y, Sikdar A, Wang D, Bradshaw WJ, et al. (2024) Characterization of covalent inhibitors that disrupt the interaction between the tandem SH2 domains of SYK and FCER1G phospho-ITAM. *PLoS ONE* 19(2): e0293548. <https://doi.org/10.1371/journal.pone.0293548>

**Editor:** Yanlin Yu, NCI: National Cancer Institute, UNITED STATES

**Received:** August 2, 2023

**Accepted:** October 15, 2023

**Published:** February 15, 2024

**Peer Review History:** PLOS recognizes the benefits of transparency in the peer review process; therefore, we enable the publication of all of the content of peer review and author responses alongside final, published articles. The editorial history of this article is available here: <https://doi.org/10.1371/journal.pone.0293548>

**Copyright:** © 2024 Bashore et al. This is an open access article distributed under the terms of the [Creative Commons Attribution License](https://creativecommons.org/licenses/by/4.0/), which permits unrestricted use, distribution, and reproduction in any medium, provided the original author and source are credited.

**Data Availability Statement:** All relevant data are within the paper and its [Supporting Information](#) file.

**1** Structural Genomics Consortium, Division of Chemical Biology and Medicinal Chemistry, UNC Eshelman School of Pharmacy, University of North Carolina at Chapel Hill, Chapel Hill, NC, United States of America, **2** Nuffield Department of Medicine, Centre for Medicines Discovery, ARUK Oxford Drug Discovery Institute, University of Oxford, Headington, Oxford, United Kingdom, **3** Department of Pharmacology and Chemical Biology, School of Medicine, Emory University, Atlanta, GA, United States of America, **4** Emory Chemical Biology Discovery Center, School of Medicine, Emory University, Atlanta, GA, United States of America, **5** Division of Chemical Biology and Medicinal Chemistry, Center for Integrative Chemical Biology and Drug Discovery, UNC Eshelman School of Pharmacy, University of North Carolina at Chapel Hill, Chapel Hill, NC, United States of America, **6** Department of Laboratory Medicine and Pathology, School of Medicine, University of Washington, Seattle, WA, United States of America, **7** Institute for Stem Cell and Regenerative Medicine, School of Medicine, University of Washington, Seattle, WA, United States of America, **8** Sage Bionetworks, Seattle, WA, United States of America, **9** The Jackson Laboratory for Mammalian Genetics, Bar Harbor, ME, United States of America

☞ These authors contributed equally to this work.

✉ Current address: Structural Genomics Consortium, Department of Medicine, Karolinska Hospital and Karolinska Institute, Stockholm, Sweden

† Members of the Emory-Sage-SGC TREAT-AD Center are provided in the Acknowledgments Section.

\* [alison.axtman@unc.edu](mailto:alison.axtman@unc.edu)

## Abstract

RNA sequencing and genetic data support spleen tyrosine kinase (SYK) and high affinity immunoglobulin epsilon receptor subunit gamma (FCER1G) as putative targets to be modulated for Alzheimer's disease (AD) therapy. FCER1G is a component of Fc receptor complexes that contain an immunoreceptor tyrosine-based activation motif (ITAM). SYK interacts with the Fc receptor by binding to doubly phosphorylated ITAM (p-ITAM) via its two tandem SH2 domains (SYK-tSH2). Interaction of the FCER1G p-ITAM with SYK-tSH2 enables SYK activation via phosphorylation. Since SYK activation is reported to exacerbate AD pathology, we hypothesized that disruption of this interaction would be beneficial for AD patients. Herein, we developed biochemical and biophysical assays to enable the discovery of small molecules that perturb the interaction between the FCER1G p-ITAM and SYK-tSH2. We identified two distinct chemotypes using a high-throughput screen (HTS) and orthogonally assessed their binding. Both chemotypes covalently modify SYK-tSH2 and

**Funding:** The research reported in this manuscript was led by the Emory-Sage-SGC TREAT-AD center and supported by grant U54AG065187 from the National Institute on Aging (NIA). The Structural Genomics Consortium (SGC) is a registered charity (number 1097737) that receives funds from Bayer Pharma AG, Boehringer Ingelheim, the Canada Foundation for Innovation, Eshelman Institute for Innovation, Genentech, Genome Canada through Ontario Genomics Institute, EU/FPPIA/OICR/McGill/KTH/Diamond, Innovative Medicines Initiative 2 Joint Undertaking, Janssen Pharmaceuticals, Merck KGaA Darmstadt Germany (aka EMD in Canada and USA), Pfizer, the São Paulo Research Foundation-FAPESP, and Takeda. The funders did not play a role in study design, data collection and interpretation, decision to publish, or manuscript preparation.

**Competing interests:** The authors have declared that no competing interests exist.

inhibit its interaction with FCER1G p-ITAM, however, these compounds lack selectivity and this limits their utility as chemical tools.

## Introduction

SYK is a key signaling kinase in adaptive and innate immunity. The 72 kDa protein is composed of a catalytic kinase domain, a flexible interdomain region B (IB), and two tandem SH2 (SYK-tSH2) domains connected by interdomain A (IA) (Fig 1A) [1]. The tandem SH2 domains of SYK bind to phosphorylated ITAM motifs such as the one on FCER1G within Fc receptor complexes (FcεRI, FcγRI, and FcγRIIIa) [2, 3]. Generation of the doubly phosphorylated ITAM (p-ITAM) is initiated by the stimulation of receptor complexes with IgE, IgG or IgM, which triggers the phosphorylation of ITAM motifs by Lyn or Fyn Src kinases (Fig 1B) [4]. SYK binds to the p-ITAM sequence region on the γ chain within Fc receptor complexes via the SYK-tSH2 domains [2]. Subsequent Lyn-mediated phosphorylation of the SYK SH2 interdomain linker region at residues Tyr348/352 leads to SYK activation [5]. Phosphorylation of the SYK activation loop at residues Tyr525/526 is reported to result in further SYK activation, as well as additional SYK autophosphorylation or transphosphorylation and direct phosphorylation by Src family kinases at Tyr residues in its interdomain A and B, kinase, and C-terminus regions [1, 6–8]. Engagement of SYK-tSH2 domains with p-ITAM releases the kinase domain from its autoinhibited state by releasing its interaction with the catalytic kinase domain [5]. SYK is not limited to Fc receptor complex interaction, as it also plays a significant role in both B cell receptor (BCR) and triggering receptor expressed on myeloid cells 2 (TREM2) signaling [9–11]. Broadly, SYK activation can initiate downstream signaling pathways such as PI3K, AKT, ERK, mTOR, NLRP3 inflammasome, among others [12–14]. These signaling pathways are proposed to play essential roles in driving AD pathology and therefore chemical probes to inhibit SYK activation are of therapeutic relevance [15–17].

Numerous ATP-competitive inhibitors that bind to the SYK kinase domain have been developed to date. These inhibitors do not disrupt the interaction between the SYK-tSH2 domain and p-ITAM on Fc receptors. ATP-competitive SYK inhibitors, entospletinib, BAY61-3606, PRT062607, and TAK-659, are potent and moderately selective [18–21]. Additional potent SYK inhibitors such as R406 are less selective, as they also potently inhibit multiple other kinases [22, 23]. Fostamatinib is the prodrug of R406 that was approved by the FDA for the treatment of chronic immune thrombocytopenia [24]. The small molecule inhibitors entospletinib, TAK-659, and cerdulatinib are in clinical trials for various cancers [25]. SYK inhibitors that exhibit good selectivity for SYK over other kinases represent useful tool compounds to interrogate SYK-mediated biology. For example, BAY61-3606 treatment or SYK knockdown with shRNA-SYK reduces phosphorylated and total tau levels *in vitro* (SH-SY5Y cells, 5 μM) and reduces p-AKT, p-mTOR, and p-p70 S6K levels [26]. Furthermore, *in vivo* mouse models of AD (Tg Tau P301S mice) showed reduced levels of phospho-tau (p-tau) and total tau (t-tau) after SYK inhibition with BAY61-3606 (20 mg/kg) over a course of 12 weeks [26]. Despite this, ATP-competitive SYK inhibitors are likely to have only limited selectivity across the human kinome and may not be suited for development as drugs for treating a chronic neurodegenerative disease such as AD. Less research has focused on inhibitors that bind to the SYK-tSH2 domain and/or that inhibit p-ITAM binding to SYK. A covalent inhibitor (1) and cysteine oxidation with hydrogen peroxide was reported to disrupt the binding of SYK-tSH2 domains with a doubly phosphorylated ITAM from a T-cell antigen receptor ζ-

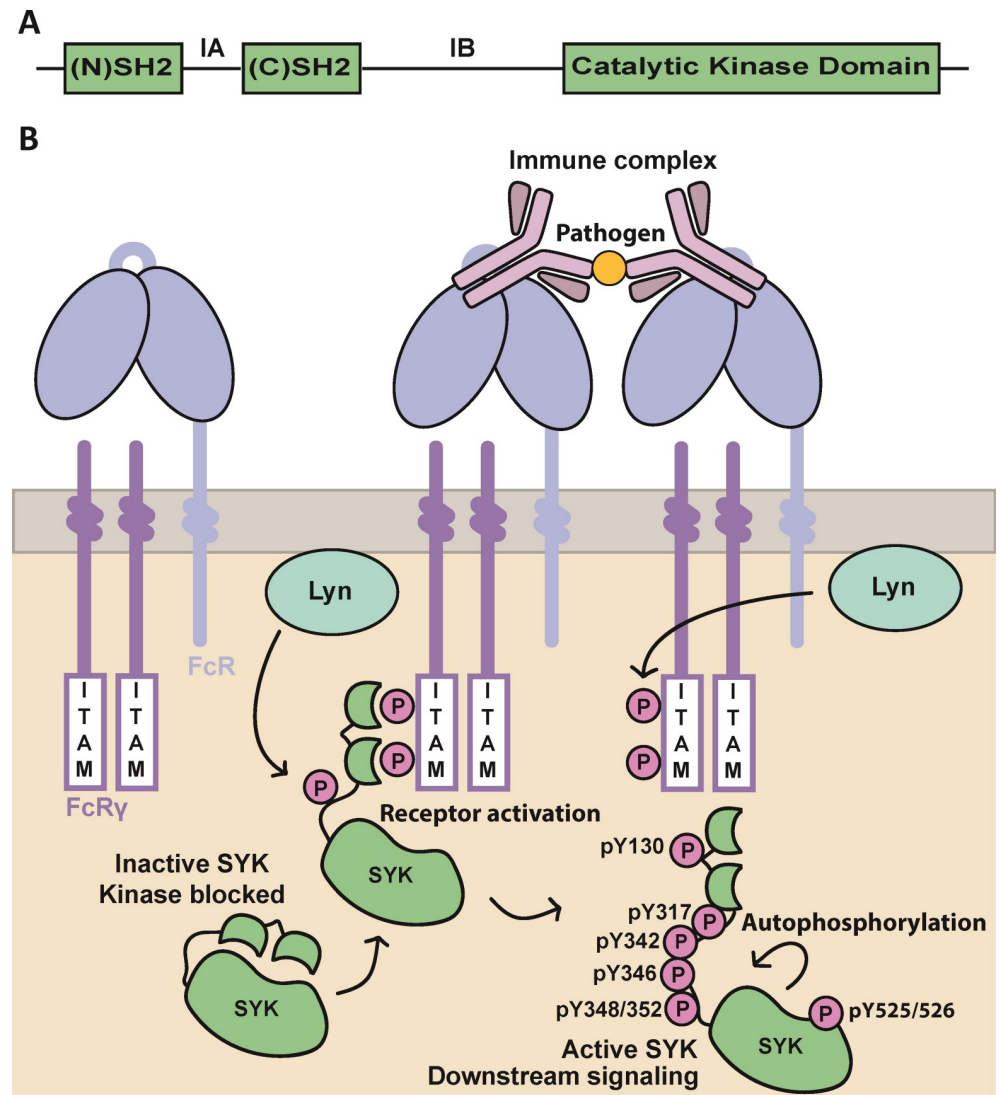


**Fig 1. SYK topology and activation mechanism with Fc receptors.** (A) Domain representation of SYK. (N)SH2 domain (residues 8–118), interdomain A (IA), (C)SH2 domain (residues 163–264), interdomain B (IB), and the catalytic kinase domain (364–620). (B) The activation mechanisms of autoinhibited SYK via both autophosphorylation and engaging p-ITAM on Fc receptors. Tyrosines phosphorylated via these mechanisms are highlighted.

<https://doi.org/10.1371/journal.pone.0293548.g001>

chain in a fluorescence polarization inhibition assay. Compound **1** binds to all 4 of the cysteines available on SYK-tSH2 as determined by mass spectrometry [27]. Cys206 was identified by the authors as the key residue for inhibition of p-ITAM binding to SYK-tSH2 domains with **1**. Mutation of Cys206 to either a serine or alanine residue resulted in a complete loss of inhibition by **1**. Cys206 is located within the (C)SH2 domain and covalent binding of this residue by **1** presumably inhibits p-ITAM binding allosterically. The authors suggest oxidation of cysteine residues in the SYK-tSH2 domain region could be a viable strategy to regulate cell signaling through SYK inhibition.

Inhibition or genetic manipulation of SYK demonstrates its importance in AD. SYK can be activated in response to A $\beta$  exposure and in turn SYK activation also correlates with increased A $\beta$  and tau hyperphosphorylation [28]. Treatment with a SYK inhibitor (BAY61-3606) in mouse tauopathy models resulted in decreased tau accumulation, neuronal and synaptic loss,

neuroinflammation, and reversed defective autophagy [15]. Additionally, SYK knockdown via shRNA mimicked pharmacological inhibition with SYK inhibitor BAY61-3606 in SH-SY5Y cells, resulting in a decrease in p-tau and t-tau levels. Inhibition of SYK with BAY61-3606 prevented lipopolysaccharide (LPS)-induced neuronal loss in primary neuron-glia cultures, and reduced microglial-mediated phagocytosis of synapses and neurons [29]. The observed decrease in microglial phagocytosis, resulting from SYK inhibition, led the authors to propose that it was the probable cause of neuroprotection. Conversely, SYK is also reported to be neuroprotective in microglia with SYK deletion causing increased A $\beta$  in mouse models of AD [16]. Phagocytosis of A $\beta$  by microglia was reduced in 5xFAD mice with SYK deletion and it is proposed that the dysregulation of GSK3 $\beta$  in the absence of SYK could be contributing to the decreased phagocytosis observed. These data suggest that further interrogating the role of SYK in AD pathology is of therapeutic relevance. FCER1G is reported to play roles in phagocytosis, microglial activation, and inflammation, which are also processes that are aberrant in AD [30, 31]. FCER1G has been previously identified as a risk gene for AD in genome-wide association studies (GWAS), and SYK was identified as being differentially expressed in an APP/PS1 (APPtg) mouse model in an age and genotype comparison despite being statistically insignificant in published GWAS [32].

Herein, we used several biochemical and biophysical assays that enable screening for small molecules that inhibit the interaction of SYK-tSH2 and the FCER1G p-ITAM. As experimental validation for pursuing the target, we first characterized the expression levels of SYK in the brain of mice in various AD models using a validated SYK antibody and examine the expression levels of SYK in human induced pluripotent stem cell (hiPSC) derived neurons and microglia. We also developed a time-resolved fluorescence energy transfer (TR-FRET) assay and a miniaturized TR-FRET assay for an ultra-high-throughput screen (uHTS) campaign to identify protein-protein interaction (PPI) disruptors. The uHTS of the Emory chemical diversity compound library, containing 138,214 compounds, identified three putative hit compounds from two orthogonal chemical series. A secondary biophysical assay, bio-layer interferometry (BLI), was used to confirm direct binding to SYK-tSH2. Intact mass analyses helped identify the active compound in one of two chemical series and confirm that all three compounds covalently modify SYK-tSH2. Importantly, these small molecules inhibit the interaction of full length SYK and FCER1G through an orthogonal chromatography-based GST pull-down (GST-PD) assay in cell lysates. We hypothesize the covalent modification of cysteine residues could be a viable strategy to disrupt the interaction of FCER1G and SYK. This strategy could help to interrogate the importance of this interaction for AD pathology.

## Results

### Bioinformatics identifies SYK and FCER1G as putative targets for AD and mRNA expression is confirmed in microglia

To prioritize putative target proteins for AD, the Emory-Sage-SGC TREAT-AD Center has developed a Target Risk Score (TRS) to prioritize putative target proteins for AD (Fig 2A and 2B) [33] and represents a composite of genetic and omic dimensions of risk. The genetic risk metric uses evidence from genetic association studies (GWAS, GWAX, and QTL), variant severity analysis, and phenotypic evidence from humans and model organisms. The multi-omic risk metric is based on signatures of differential expression from meta-analyses of transcriptomic and proteomic data from the AMP-AD consortium.

The TRS for SYK is 3.84, which places SYK in the 97<sup>th</sup> percentile of all scored targets. SYK is found to be differentially expressed in brains of AD patients relative to controls in both transcriptomic and proteomic studies, giving it an omics score of 1.98 out of 2. The genetic

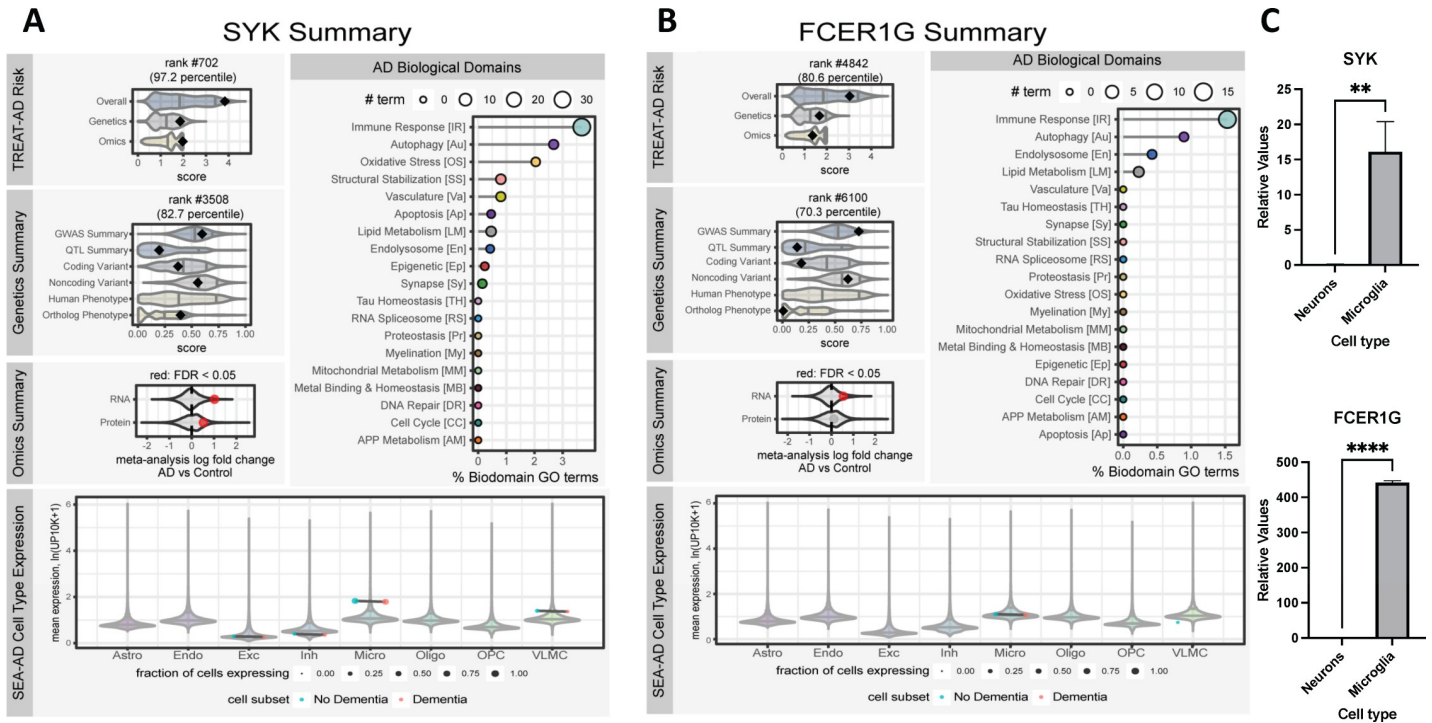


**Fig 2.** TREAT-AD bioinformatic summaries for SYK (A) and FCER1G (B). For each target, the composite Target Risk Score (Overall, top left) is a sum of the Genetics and Omics risk dimensions. The Genetics Summary includes the average rank of gene-level significance values from GWAS and QTL studies, variant severity analysis, and phenotype summaries for both human genes (Hsap) and orthologous genes. The Omics Summary represents the results from meta-analyses of AMP-AD transcriptomic and proteomic datasets showing the effect size (log fold change) and significance (red points are detected at an FDR < 0.05). For all plots no point plotted indicates that the gene was not scored or measured in that dimension. The AD Biological Domains shows the fraction of all terms annotated to a biological domain to which the gene is annotated, and the size of the point indicates the number of terms. The SEA-AD Cell Type Expression panel shows the mean expression values for the gene per cell subclass, stratified by cognitive status of the donor, where expression is measured as the natural log [number of unique molecular identifiers (UMIs) for each gene in a given cell divided by the total number of UMIs in the same cell divided by 10,000] plus 1. The size of each point represents the fraction of cells from each cell type expressing the gene. (C) mRNA expression levels of SYK and FCER1G in hiPSC-derived neurons and microglia.

<https://doi.org/10.1371/journal.pone.0293548.g002>

contribution to the SYK TRS is 1.86 out of 3 (82<sup>nd</sup> percentile), which is based on modest and consistent scores from the association studies (GWAS and QTL) as well as variant severity analyses, as well as a high correspondence of phenotypes attributable to SYK orthologs in model organisms and AD related phenotypes.

The TRS for FCER1G is slightly lower than that for SYK at 3.03 (80<sup>th</sup> percentile). FCER1G is only found to be significantly differentially expressed based on meta-analyses of transcriptomic datasets, leading to a slightly lower omics risk score of 1.36 out of 2. The genetics risk computed for FCER1G is also less than SYK—1.67 out of 3—despite having a relatively higher GWAS summary metric, owing in large part to a lower contribution from coding variant severity and a lower correspondence between FCER1G ortholog phenotypes and AD.

The Emory-Sage-SGC TREAT-AD Center has also developed the Biological Domains of AD as an approach to objectively define and categorize disease relevant risk. There are 19 distinct biological domains derived from various molecular endophenotypes that have been linked with AD, which are defined functionally by largely non-overlapping sets of Gene Ontology (GO) terms. Both SYK and FCER1G have the strongest annotation to the Immune Response and Autophagy biological domains. Finally, to understand the relevant cell types for each gene, summary expression from the SEA-AD snRNA-seq dataset was considered [34]. Expression of both SYK and FCER1G is detected broadly in microglia. The mRNA levels of SYK and FCER1G were measured in hiPSC derived neurons and microglia (Fig 2C).

Significantly higher levels of both SYK and FCER1G were quantified in microglia compared to neurons, which is consistent with the reported roles of the activation of SYK and FcγR in microglia [35].

### Identification of covalent inhibitors of the interaction between FCER1G p-ITAM and SYK-tSH2 via HTS

To facilitate identification of inhibitors of the SYK-FCER1G interaction, we developed a TR-FRET assay using recombinant protein comprising the tSH2 domain of SYK (residues M6-N269) fused to an N-terminal 6×His tag (S1A Fig). The TR-FRET assay is based on the interaction of a FITC-labeled FCER1G p-ITAM peptide to the 6×His-SYK-tSH2 protein in complex with a terbium-conjugated anti-His antibody (Tb-Ab) (Fig 3B). Once excited, a TR-FRET signal is generated from the Tb donor to the FITC acceptor fluorophore. The TR-FRET signal produced by this interaction can be competed in a dose-dependent manner by the addition of unlabeled FCER1G p-ITAM peptide ( $IC_{50} = 12$  nM). As expected, the non-phosphorylated FCER1G ITAM peptide has no effect on the TR-FRET signal ( $IC_{50} > 1000$  nM, Fig 3C). To enable uHTS for large scale screening of small molecule libraries, we miniaturized the TR-FRET assay from 96-well plate format to a 1536-well. A primary screen of 138,214 small molecules from the Emory Chemical Biology Discovery Center (ECBDC)

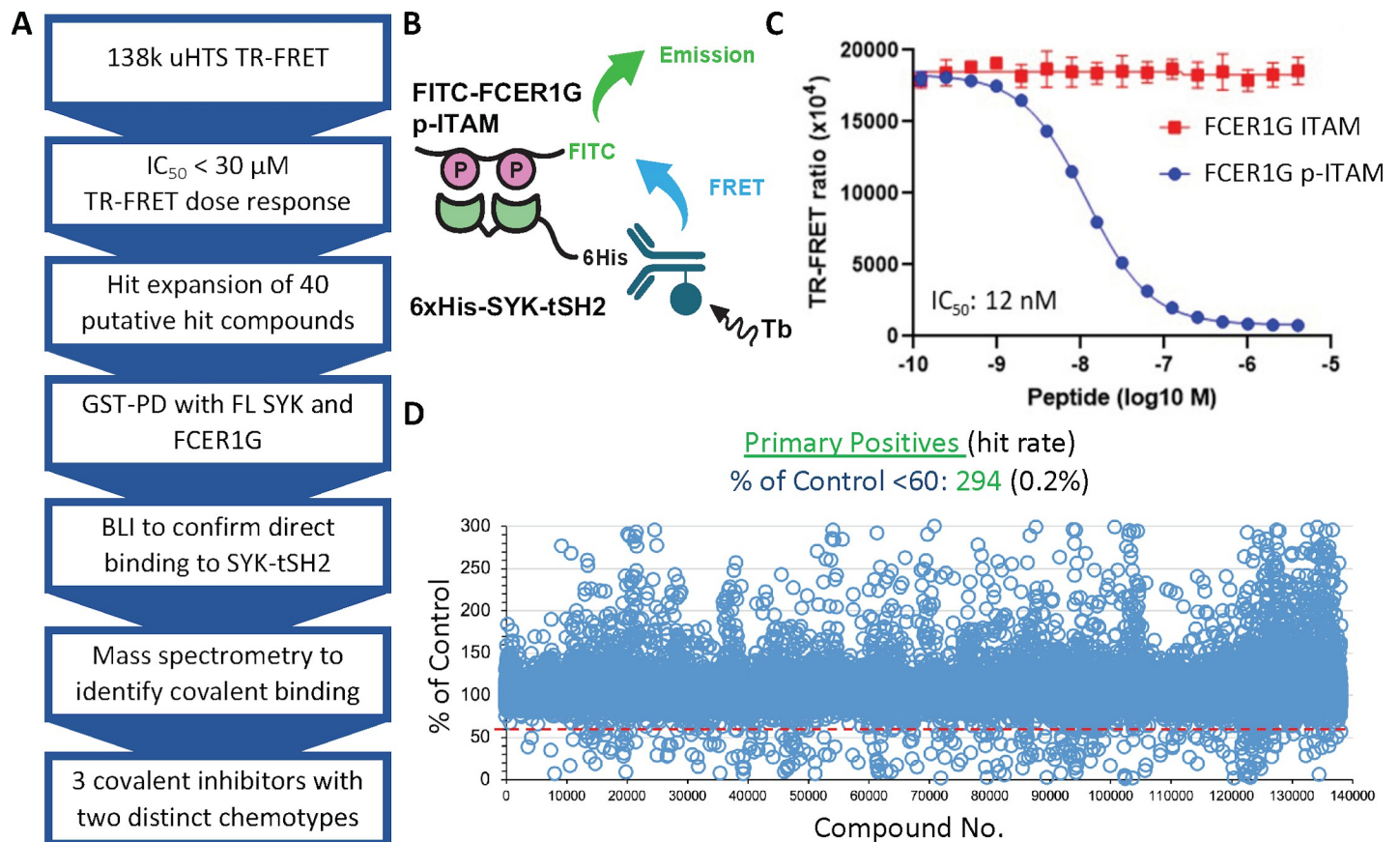


**Fig 3. Compound screening cascade and the development and use of a biochemical TR-FRET assay to evaluate inhibition of the PPI between SYK-tSH2 and the FCER1G p-ITAM peptide.** (A) Compound screening cascade. (B) and (C) TR-FRET assay with 6xHis-SYK-tSH2 and a p-ITAM-FITC tagged peptide. Unlabeled FCER1G p-ITAM can displace p-ITAM-FITC, while FCER1G ITAM does not. (D) Primary uHTS of 138,214 compounds with 294 primary positive identified.

<https://doi.org/10.1371/journal.pone.0293548.g003>

identified 294 primary positives in which the signal was less than 60% of the control, corresponding to a hit rate of 0.2% (Fig 3D). The 294 putative hits were confirmed in a dose-response format from the library stock plates and 135 compounds were confirmed to have an  $IC_{50} < 20 \mu M$ . Of these 135 small molecules, 112 were commercially available for re-evaluation in the primary TR-FRET assay, leading to confirmation of 54 compounds with  $IC_{50} < 30 \mu M$ . This set of 54 potential leads was counter-screened in a TR-FRET assay developed for an unrelated PPI (moesin-CD44) with the same donor and acceptor fluorophores in order to exclude fluorophore interference compounds [36, 37]. After removing pan-assay interference compounds (PAINS) and cross-reactive compounds from the moesin-CD44 assay, 40 compounds were progressed for further hit validation in a panel of secondary assays. These compounds were triaged first in a GST-PD assays with full length SYK and FCER1G, followed by confirmation in a biophysical assay to determine direct binding.

Pull-down assays were used as an orthogonal assay to determine if the compounds could disrupt the PPI between full length SYK and FCER1G proteins from cell lysates. To optimize GST pull-down assays, full length GST-SYK and FCER1G-Flag were co-expressed in HEK293

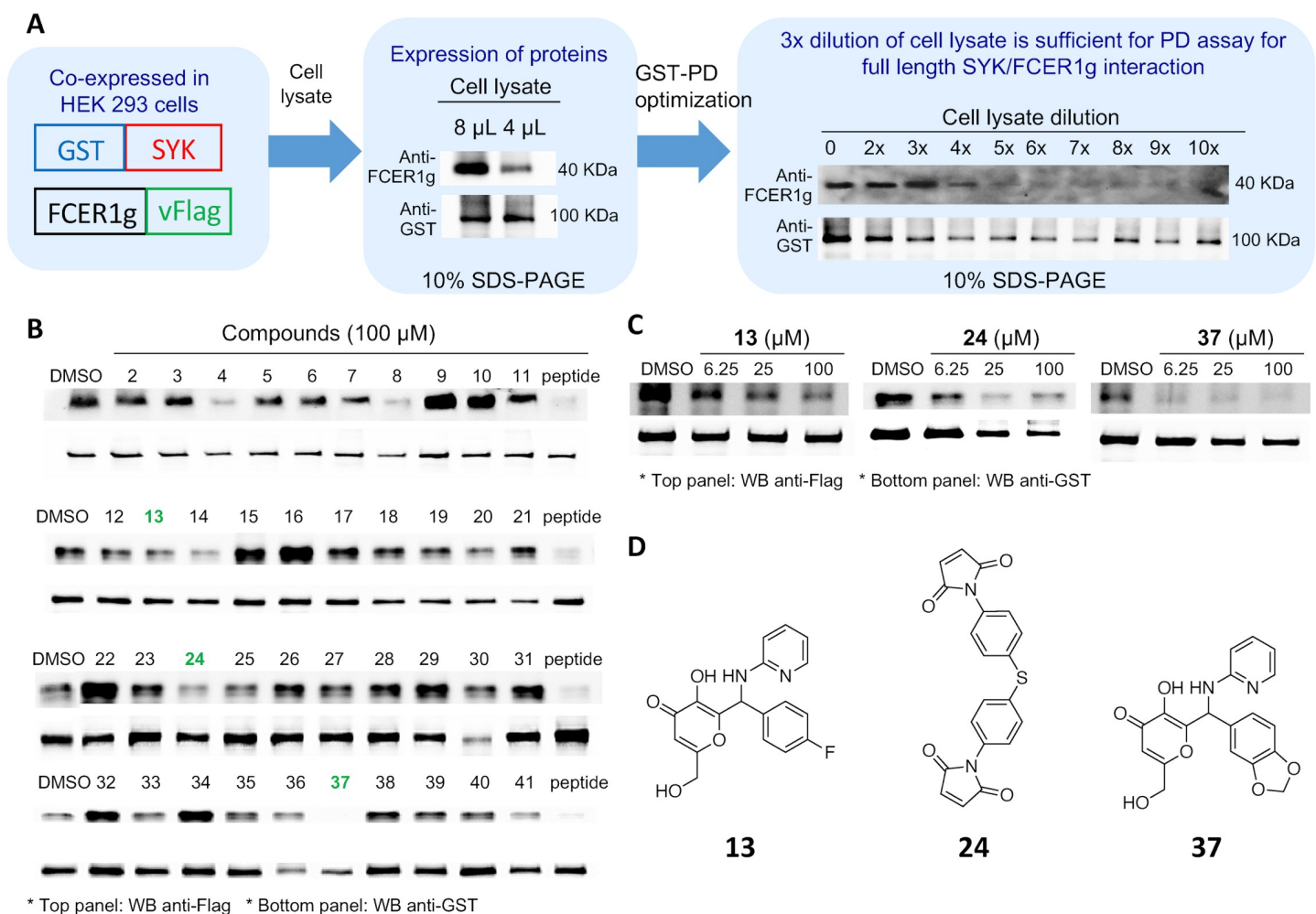


**Fig 4. Identification of 3 compounds that inhibit the interaction of SYK and FCER1G in a GST-SYK and FCER1G-Flag pull-down assay.** (A) Optimization of the GST-SYK and FCER1G-Flag pull-down assay in HEK293 cells. (B) Compounds 13, 24, and 37 were able to inhibit the interaction between SYK-GST and FCER1G-Flag in a pull-down assay at a single concentration (100  $\mu M$ ). (C) Compounds 13, 24, and 37 were tested via GST-pull-down in a dose-response fashion. (D) Chemical structures of compounds 13, 24, and 37. Unmodified blots corresponding with panels (A), (B), and (C) are included in S7 Fig.

<https://doi.org/10.1371/journal.pone.0293548.g004>

cells prior to lysis and the protein expression and cell lysate concentrations tested (Fig 4A). All 40 compounds that progressed from uHTS were tested via GST-PD at a single concentration (100  $\mu\text{M}$ ) to determine if they could inhibit the PPI between the full-length proteins, with the p-ITAM FCER1G peptide used as a positive control (Fig 4B). Among the 40 compounds tested for PPI disruption at 100  $\mu\text{M}$ , 11 compounds inhibited the primary GST-PD at 100  $\mu\text{M}$ , and 5 of these 11 compounds (4, 13, 24, 32, and 37) were confirmed to disrupt the PPI in a dose-response format. Compounds 13, 24, and 37 showed the greatest PPI disruption in the dose-response format (Table 1 and Fig 4C). Compound 24 contains a promiscuous maleimide, which is well known to react indiscriminately with proteins. Compound 4 had poor solubility (25  $\mu\text{M}$ ), with both 4 and 32 displaying inconsistent GST-PD data (Figs 4B and S2A and S2B). Therefore, these compounds were not progressed further.

To validate direct binding of hit compounds 13, 32, and 37 to SYK-tSH2, we performed an orthogonal biophysical protein-small molecule direct binding assay, BLI. A biotinylated version of SYK-tSH2 (SYK-tSH2-c022; residues M6-269) was used, which lacked the 6xHis tag (S1C Fig). Compounds 13 and 37 were shown to bind to SYK-tSH2 with  $K_D$  values of 8.4  $\mu\text{M}$  and 10.3  $\mu\text{M}$ , respectively (Table 1 and S3 Fig). In addition to the inconsistent GST-PD results previously mentioned, compound 32 did not bind to the SYK-tSH2 domains and therefore it was not progressed further.

### Compounds 13 and 37 covalently modify SYK-tSH2

The HTS hits 13 and 37 contain a kojic acid moiety, which is proposed to react covalently with proteins in the literature [38]. As a result, we thought that it was likely these compounds are also reacting covalently with SYK-tSH2. Compounds 13 and 37 were incubated with SYK-tSH2 at 100  $\mu\text{M}$  for 1 h at room temperature and a covalent reaction was revealed by mass spectrometry (Fig 5A). When bound to the protein, these kojic acid-derived compounds have a 94 Da decrease in mass due to the loss of the pyridin-2-amine leaving group to reveal a Michael acceptor that can react covalently with cysteine residues (Fig 5B). 13 and 37 formed between one and five and between two and seven mass adducts of 248 and 274 Da respectively, suggesting that these compounds react indiscriminately with cysteine residues and likely other nucleophilic amino acid residues due to the mass adducts observed totaling above the number of available cysteines (4).

### Hit expansion of 40 putative hits leads to identification of thiouric acid compounds that covalently modify SYK-tSH2 via oxidative disulfide bond formation

To expand on the initial 40 putative hits that were identified via uHTS (Fig 3D), additional commercially available structural analogues were ordered and screened via TR-FRET and

**Table 1. Biochemical and biophysical data for compounds 37, 13, 42, 43, and 44.** The estimated  $\text{IC}_{50}$  for GST-PD is calculated via the western blot densitometry. <sup>a</sup> Solubility calculated with a nephelometer (S5 Fig). <sup>b</sup> Kinetic solubility calculated by Analiza, Inc. An unmodified blot used to generate GST-PD  $\text{IC}_{50}$  values is included in S7 Fig.

ID	GST-PD estimated $\text{IC}_{50}$ ( $\mu\text{M}$ )	BLI $K_D$ ( $\mu\text{M}$ )	Solubility ( $\mu\text{M}$ )
37	1	8.4 $\pm$ 0.3	100 <sup>a</sup>
13	6	10.3 $\pm$ 0.3	100 <sup>a</sup>
44	16	4 $\pm$ 0.2	70.9 <sup>b</sup>
42 (fresh DMSO stock)	NT	99 $\pm$ 0.8	208 <sup>b</sup>
43	NT	NB	NT

<https://doi.org/10.1371/journal.pone.0293548.t001>



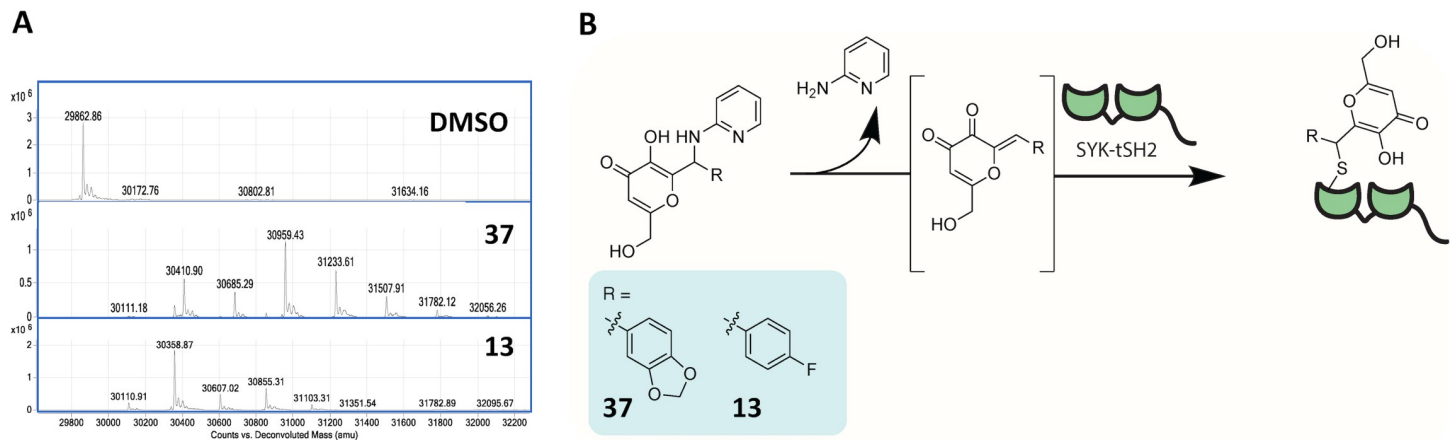


**Fig 5. Compounds 13 and 37 react covalently with SYK-tSH2.** (A) Mass spectrometry analysis of SYK incubated with compounds 37 and 13 at 100  $\mu$ M for 1 h at room temperature. (B) Hypothesized mechanism of inhibition of 37 and 13 with SYK-tSH2.

<https://doi.org/10.1371/journal.pone.0293548.g005>

differential scanning fluorimetry (DSF) (S1 Table). Two analogues of primary hit **39** ( $IC_{50}$  = 27.7  $\mu$ M) from uHTS, compounds **42** and **43** (Fig 6A and 6B), significantly destabilized SYK-tSH2 protein in the DSF assay and demonstrated single-digit micromolar  $IC_{50}$  values in the TR-FRET assay (S1 Table). **43** is a close analogue of the primary hit **39**, varying only in methylation of the imide nitrogen versus **39**, and demonstrated a TR-FRET  $IC_{50}$  of  $3.0 \pm 1.7$   $\mu$ M and a DSF  $\Delta T_m$  of  $-6.7 \pm 0.4$   $^{\circ}$ C. Strikingly, compound **42**, which also contains a methylated imide nitrogen but lacks the isopropyl group on the thiourea nitrogen versus **39**, demonstrated a TR-FRET  $IC_{50}$  of  $1.9 \pm 0.20$   $\mu$ M and a DSF  $\Delta T_m$  of  $-17 \pm 0.3$   $^{\circ}$ C (S1 Table). The observation of a substantial reduction in protein melting temperature motivated us to determine if the compounds interacted covalently with the SYK-tSH2 domains. Additionally, since the thiourea in these small molecules is reported to react via oxidation, the compounds could be capable of forming a covalent disulfide bond with cysteine residues on SYK [39]. We used compound **1**, which is a known covalent modifier of SYK-tSH2, as a positive control in the mass spectrometry analysis [27]. Compound **1** could not be used as a positive control in the TR-FRET due to assay interference with the compound quenching the TR-FRET donor signal. Compound **1** formed one or two  $\times$  222 Da adducts with the protein, suggesting that under these experimental conditions **1** reacts with either one or two cysteine residues covalently. Incubation of **42** and **43** at 100  $\mu$ M for 1 h with SYK-tSH2 revealed that only compound **42** covalently modifies SYK-tSH2, but oddly only with older DMSO stock solutions (Fig 6C). Despite the similar structures, **43** did not demonstrate covalent attachment. Adducts of two (422 Da) more than the protein mass after **42** incubation suggests that this compound is binding at two cysteine residue sites on the protein surface (Fig 6C). Confoundingly, mass spectrometry analysis of SYK-tSH2 with a freshly prepared DMSO stock of **42**, however, did not result in the previously observed mass adduct (Fig 6C). Analytical characterization of freshly prepared solutions of **42** and **43** versus the older DMSO stocks that had been used in the preliminary mass spectrometry analyses revealed that the compounds were monomeric when freshly dissolved but had formed corresponding disulfide dimers in DMSO over time (S4 Fig). The freshly prepared DMSO stock solution of **42** did not form a covalent adduct (Fig 6D). Literature reports support that this type of chemical reaction can occur in DMSO, forming a disulfide bond [40, 41]. The proposed active disulfide compound, **44**, was synthesized from **42** by heating it in DMF at 100  $^{\circ}$ C and then purifying via aqueous filtration (Fig 6B) [42]. **44** exhibits poor organic solubility and, accordingly, its melting point temperature is  $>300$   $^{\circ}$ C [43, 44]. The kinetic solubility of **44** was

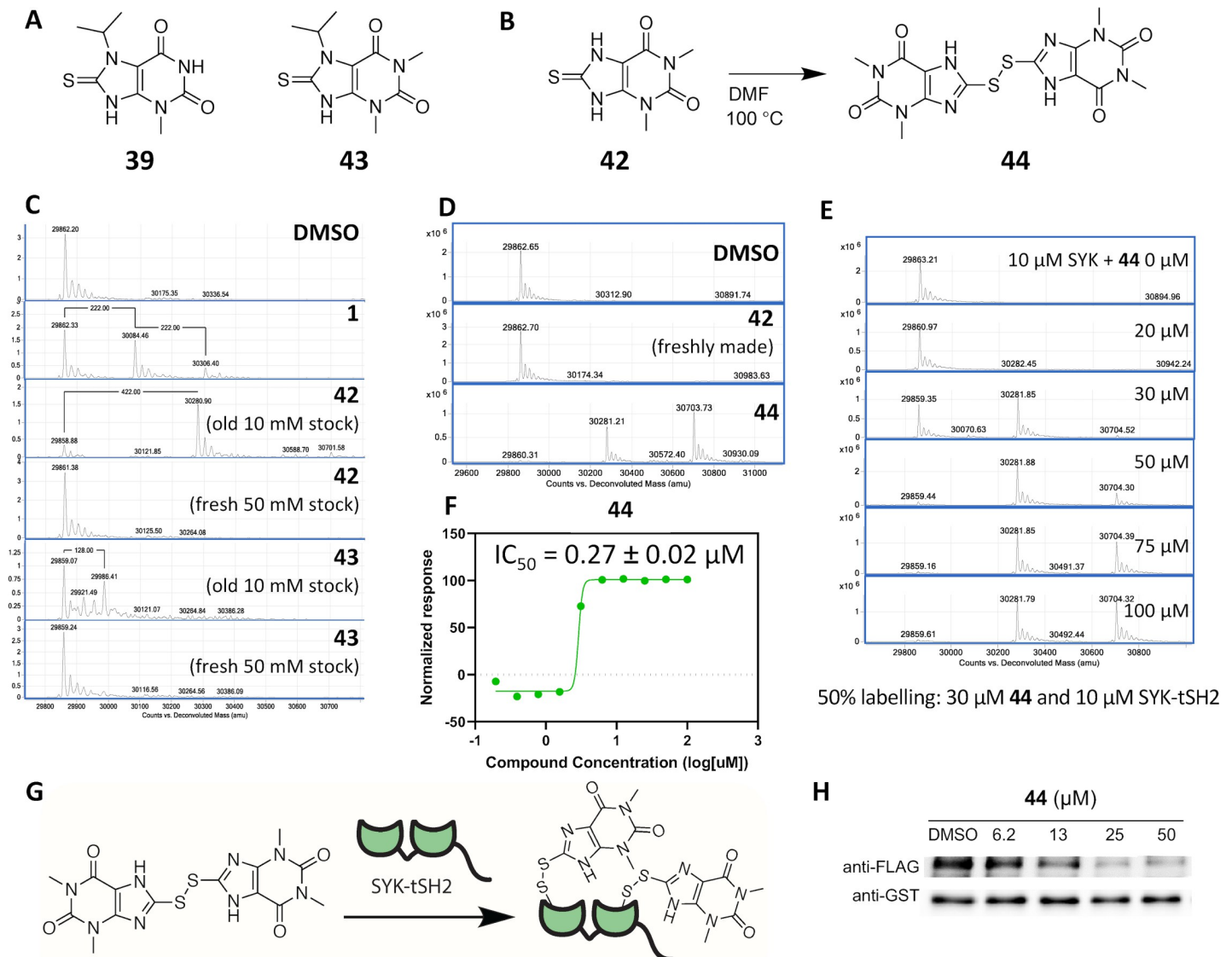


**Fig 6. Compound 44 covalently modifies SYK-tSH2.** (A) Chemical structures of initial HTS hit **39** and analogue **43**. (B) Synthesis of **44** from analogue **42**. (C) Mass spectrometry of SYK-SH2 incubated with covalent inhibitor **1** and old versus fresh stocks of **42** and **43** at 100  $\mu$ M for 1 h at room temperature. Only the old DMSO stock of **42** reacts covalently with SYK-tSH2. (D) Mass spectrometry of SYK-tSH2 incubated with **42** and **44** at 100  $\mu$ M for 1 h at room temperature. (E) Dose-response of **44** in covalently labelling SYK-tSH2, assessed by mass spectrometry. (F) Dose response curve of **44** in the TR-FRET assay ( $IC_{50} = 0.27 \pm 0.02 \mu$ M). (G) Hypothesized mechanism of inhibition of **44** with SYK-tSH2. (H) Compound **44** disrupted the PPI via GST-pulldown in a dose-response fashion. An unmodified blot corresponding with panel (H) is included in S7 Fig.

<https://doi.org/10.1371/journal.pone.0293548.g006>

measured as 70.9  $\mu$ M, which as expected is less soluble than the monomer **42** at 208  $\mu$ M, however, is in a reasonable range of solubility (Table 1). Like we had originally observed for the older DMSO stock solution of **42** (Fig 6C), **44** forms two to four mass adducts (422 Da and 844 Da) more than the protein mass when incubated SYK-tSH2 for 1 h (Fig 6D). Since the freshly made DMSO stock solutions of **42** did not covalently modify SYK-tSH2, we propose that it forms disulfide **44** over time and this disulfide compound is responsible for the observed activity. Additionally, **44** was potent in the TR-FRET assay, demonstrating an  $IC_{50} = 0.27 \pm 0.02 \mu$ M (Fig 6F). When **44** was analyzed by mass spectrometry in dose-response format, it exhibited 50% labelling of 10  $\mu$ M SYK-tSH2 at 30  $\mu$ M **44** (Fig 6E). Due to the mass

adducts of two to four (422 Da and 844 Da), we propose that **44** is forming a disulfide bond with between two or four cysteines on SYK-tSH2 (Fig 6G).

To confirm binding to SYK-tSH2 domains via an orthogonal assay the compounds **42** (as a fresh DMSO stock containing only the monomer), **43** and **44** were analyzed by BLI (Table 1 and S3 Fig). **44** demonstrated slightly more efficacious binding to SYK-tSH2 than the compounds identified from the HTS screen (**13** and **37**), with a  $K_d = 4.0 \mu\text{M}$  (Table 1). Compound **42** was also evaluated via BLI as a fresh DMSO stock, which should only contain the monomeric compound, and did not bind to the protein ( $K_d = 99 \mu\text{M}$ ). Finally, consistent with the mass spectrometry analysis (Fig 6C), **43** did not bind to SYK-tSH2 when analyzed via BLI (Table 1). Additionally, compound **44** was able to disrupt the full-length interaction of SYK and FCER1G via a GST-PD assay (Table 1 and Fig 6H).

### Compounds 13, 37, and 44 lack selectivity for SYK-tSH2

Mass spectrometry was used to determine the selectivity of the compounds identified as covalent inhibitors of SYK-tSH2 (**13**, **37**, and **44**) against a select panel of proteins. Proteins MSN, TBXT, and SHIP1 were used for this experiment due to the knowledge that they contain accessible cysteines that have been targeted for prior covalent compound screening. The compounds were incubated at a concentration of 100  $\mu\text{M}$  with the respective protein for 1 h at room temperature (Fig 7). As previously shown herein (Figs 5 and 6 and S6), compounds **13**, **37**, and **44** form covalent mass adducts with SYK protein. **44** incubated with TBXT, which has two available cysteines, forms two mass adducts (420 Da). Compounds **13** and **37** both form two or three mass adducts, suggesting that the compound does not exclusively covalently react with cysteines on TBXT and reacts with additional residues. MSN, which has four available cysteines for modification, only forms two mass adducts (420 Da) with **44**. Intriguingly, compounds **13** and **37** only form one weak mass adduct with MSN (248 and 274 Da, respectively), with protein predominantly unlabeled by the two compounds. **44** was incubated at a lower concentration of 30  $\mu\text{M}$  with SYK, TBXT, and MSN and resulted in the same formation of mass adducts as 100  $\mu\text{M}$  incubation (S6A, S6C and S6D Fig). Additionally, **44** was incubated with SHIP1, which has 10 available cysteine residues, and forms mass adducts of 8 or 10 (1678 or 2101 Da) (S6B Fig). Collectively these data indicates that **13**, **37**, and **44** bind covalently to available cysteines on distinct proteins indiscriminately. Furthermore, compounds **13**, and **37** show mass adducts which are greater than the number of available cysteines, suggesting the potential for more promiscuous binding with amino acid residues.

### Discussion

Herein, we describe the design and utilization of several biochemical and biophysical assays aimed at identification of inhibitors of the PPI between SYK-tSH2 and the FCER1G phospho-ITAM. As this interaction promotes activation of SYK and activated SYK has been implicated as a driver of AD pathology, pharmacological inhibition of this PPI is proposed to slow AD progression. Furthermore, SYK expression is elevated in AD-relevant regions of the brain in AD mouse models. We employed a biochemical TR-FRET assay as a high-throughput approach to identify putative PPI inhibitors. Since TR-FRET is an indirect method of detection, BLI, an orthogonal biophysical assay was enlisted to demonstrate direct binding of the inhibitors to SYK-tSH2. Mass spectrometry analysis confirmed that binding to SYK-tSH2 was covalent for some compounds (**13**, **37**, and **44**), but not others (**42** and **43**). GST-PD assays confirmed that the PPI disruption was maintained when full length rather than truncated proteins was employed for these compounds.

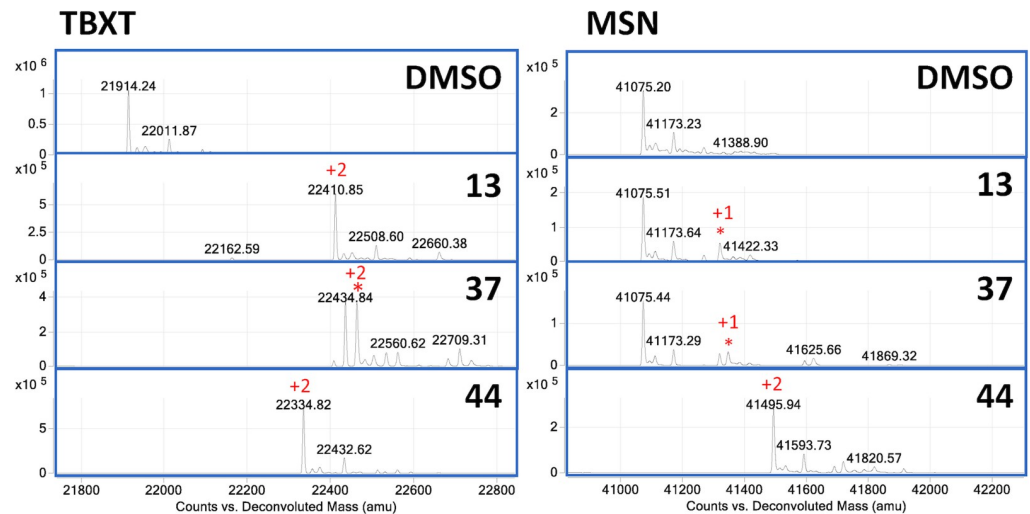


**Fig 7. Compounds 13, 37, and 44 (100  $\mu$ M) bind covalently to TBXT and MSN via mass spectrometry.** Number of mass adducts of the compound are indicated in red.

<https://doi.org/10.1371/journal.pone.0293548.g007>

We noted slight discrepancies in the data generated using the different assays. The TR-FRET assay identified many single-digit micromolar inhibitors of our PPI, including those compounds found in Tables 1 and S1. However, not all of these were confirmed to bind to SYK-tSH2 via the BLI orthogonal biophysical assay and GST-PD assays. Most compounds pursued for further studies displayed at least single-digit micromolar potency in the TR-FRET assay. Generally, compounds that showed potent binding to SYK-tSH2 via BLI reacted covalently with the protein as assessed by mass spectrometry.

When structurally similar analogs of 39 were analyzed via DSF (S1 Table), significant destabilization of SYK-tSH2 was observed with compounds 42 and 43, and the most destabilizing compounds corresponded to the most potent TR-FRET value. Significant destabilization observed in the DSF assay motivated examination of a potential covalent mechanism of binding. Compound 42 (an old DMSO solution, mostly containing 44) was shown to bind covalently to SYK-tSH2. However, compound 43 did not form a mass adduct corresponding to compound addition, despite the destabilizing DSF value. We found that compounds 42 and 43 form a disulfide in DMSO solution, which is responsible for the increased mass observed and covalent inhibition of SYK-tSH2. Evaluation of analogs of the initial HTS hit (39) led us to compound 44, which was discovered to be the active component in older DMSO stocks of 42. Monomeric 42 had formed a disulfide compound over time in DMSO, resulting in formation of 44. 44 has sub-micromolar potency in the TR-FRET assay, weak micromolar potency via BLI, and inhibited the GST-PD assay with weaker double-digit micromolar estimated  $IC_{50}$  values. The observed poor solubility of 44 compared to the monomeric 42 in DMSO leads us to propose that the chemotype suffers from solubility issues, which were magnified when moving into cellular lysate for GST-PD experiments. These compounds were found to have good aqueous solubility without any noted precipitation and yield different kinetic solubility values (Table 1), suggesting that 42 did not completely transform into 44 in a mostly aqueous solution when incubated overnight. We propose that for all DMSO stocks containing the thiouric acid moiety found in 42 and 43 a percentage of the compound present will have formed the disulfide compound. In support of this reactivity, 42 is often used as a reactant in the synthesis of more elaborate compounds due to the oxidative nature of its sulfur atom [39, 45]. We propose that the isopropyl group on 43 reduces its ability to form the active disulfide species as

efficiently as **42** and/or that it exists in a dynamic equilibrium with its monomeric counterpart. A structurally similar analog of **42**, 8-thiouric acid, was co-crystallized with urate oxidase (UOX, PDB code: 3LBG) and demonstrated both non-covalent binding of the monomeric compound and a covalent disulfide bond formed between the monomeric compound and Cys35 [46]. It is possible that the covalent modification of UOX was executed by a dimeric form of 8-thiouric acid, similar to what we observed for **42**, forming **44** and then labeling SYK-tSH2 (Fig 6G). Despite the covalent nature of these inhibitors, promisingly we did not observe indiscriminate binding to the cysteines on SYK-tSH2, with only two to four mass adducts observed up to a concentration of 100  $\mu\text{M}$ .

Compounds **13** and **37** that were identified from the primary HTS share the same chemotype, which contains a kojic acid derived core scaffold. **13** and **37** consistently exhibited single-digit micromolar values in TR-FRET, BLI, and GST-PD assays. The chemotype for these compounds is different to compound **44** and compound **1**, which bind via an oxidative disulfide and covalent aromatic substitution mechanism, respectively. Inhibitors containing the kojic acid core modify an unrelated protein-transcriptional enhanced associate domain (TEAD) [38]. The reported mechanism that these compounds react with TEAD involves an initial retro Mannich reaction, revealing a Michael acceptor that can react covalently with an available cysteine residue on the protein (Fig 5B). Compounds **13** and **37** bind to cysteine(s) on SYK-tSH2, resulting in potent inhibition of our PPI. Multiple adducts are observed with these compounds, further suggesting that the compounds will likely bind promiscuously to readily available cysteine residues. Early identification of this indiscriminate labeling of another protein diminished our enthusiasm for these hits.

While **13**, **37**, and **44** are confirmed to inhibit the PPI between SYK-tSH2 and the FCER1G peptide with micromolar potency, the selectivity of these small molecules is poor via mass spectrometry. Despite **44** binding to fewer amino acid residues on SYK-tSH2 than **13** and **37** observed by mass spectrometry, against a select panel of proteins with known available cysteines, no selectivity was observed. Despite the success inhibiting the PPI between SYK and FCER1G peptide, it is clear that more work needs to be pursued to improve the selectivity of these compounds. These compounds require further optimization to become good tools for interrogating the function of SYK and FCER1G in a cellular context and should only be used with caution.

## Conclusion

We have identified three confirmed covalent inhibitors of SYK-tSH2 domain (**13**, **37**, and **44**) that disrupt its interaction with the FCER1G peptide when used at micromolar concentrations. These compounds bind to SYK-tSH2 when evaluated using biophysical methods and mass spectrometry. Additionally, they inhibit the interaction between full length SYK and FCER1G. These compounds highlight that covalent inhibition of SYK-tSH2 is a viable strategy to assess the implications of inhibiting the PPI between SYK and FCER1G. Intriguingly, we have identified covalent inhibition of SYK-tSH2 via two distinct mechanisms to that of compound **1**, which reacts via a covalent aromatic substitution reaction with cysteine. Cysteine reacts via a Michael addition on the alkene revealed on compounds **13** and **37**. The compounds undergo an initial retro Mannich reaction that generates the alkene, which is the reactive Michael acceptor species for covalent inhibition. With compound **44**, which is a disulfide compound, an oxidative reaction occurs forming a disulfide with an available cysteine residue. We have highlighted some limitations related to the reactivity of the kojic acid core shared by **13** and **37** and the disulfide containing compound **44** with proteins unrelated to SYK. In addition, the observed sub-optimal solubility of **44** in organic solution as well as poor selectivity for the

SYK-FCER1G interface limits its utility. These compounds or close structural analogs that share the same chemical liabilities are exemplified hits from other programs. Our learnings should be considered when advancing these small molecules as chemical leads. Overall, we have demonstrated that the interaction between these two proteins can be disrupted via small covalent molecules that utilize distinct covalent mechanisms, identifying this strategy as a potential alternative approach towards the development of small molecule regulators of SYK signaling.

## Materials and methods

### Plasmid constructs and peptides

Expression plasmids used in protein purification were generated by PCR amplification of the tandem SH2 domains of human SYK (residues M6-N269) from the Mammalian Gene Collection cDNA library (IMAGE:3870426). The PCR product was cloned into the *E. coli* expression vector pNIC28-Bsa4 or pNIC-Bio3 using ligation independent cloning. Cloning into both vectors gives rise to an N-terminal fusion of SYK with a 6xHis tag and a TEV protease cleavage site (SYKA-c020), while the pNIC-Bio3 construct contains in addition a C-terminal AviTag fusion. TR-FRET assays were performed using an FITC-conjugated peptide containing the FCER1G ITAM sequence with two phosphotyrosines (FCER1G-phospho-ITAM[62–81]-FITC: DGV(pY)TGLSTRNQET(pY)ETLKH-FITC). A non-phosphorylated ITAM sequence was used as a control (FCER1G-nonphospho-ITAM[62–81]-FITC: DGVYTGLSTRNQE-TYETLKH-FITC). Biophysical assays employed a phosphorylated ITAM without FITC conjugation (FCER1G-phospho-ITAM[62–81]: DGV(pY)TGLSTRNQET(pY)ETLKH). Peptides were custom synthesized by LifeTein.

GST-, VF-tagged human SYK and FCER1G plasmids for mammalian expression were generated using Gateway cloning technology (Invitrogen) as described previously [47]. The DNA was purified using ZymoPURE Plasmid Maxiprep Kit (D4203, Zymo Research).

### iPSC data

iPSCs were cultured and differentiated to neurons and microglia as previously described [48, 49]. For neuronal differentiation, iPSCs were plated on Matrigel coated 6-well plates at a density of 3.5 million cells per well and fed with Basal Neural Maintenance Media (1:1 DMEM/F12 + glutamine media/neurobasal media, 0.5% N2 supplement, 1% B27 supplement, 0.5% GlutaMax, 0.5% insulin-transferrin-selenium, 0.5% NEAA, 0.2%  $\beta$ -mercaptoethanol; Gibco) + 10mM SB-431542 + 0.5mM LDN-193189 (Biogems). Cells were fed daily for seven days. On day eight, cells were incubated with Versene, gently dissociated using cell scrapers, and passaged at a ratio of 1:3. On day nine, media was switched to Basal Neural Maintenance Media and fed daily. On day 13, media was switched to Basal Neural Maintenance Media with 20 ng/mL FGF (R&D Systems) and fed daily. On day sixteen, cells were passaged again at a ratio of 1:3. Cells were fed until approximately day 23. At this time, cells were FACS sorted to obtain the CD184/CD24 positive, CD44/CD271 negative neural precursor cell (NPC) population. Following sorting, NPCs were expanded for neural differentiation. For cortical neuronal differentiation, NPCs were plated out in 10cm cell culture dishes at a density of 6 million cells/10 cm plate. After 24 h, cells were switched to Neural Differentiation media (DMEM-F12 + glutamine, 0.5% N2 supplement, 1% B27 supplement, 0.5% GlutaMax) + 0.02  $\mu$ g/mL brain-derived neurotrophic factor (PeproTech) + 0.02  $\mu$ g/mL glial-cell-derived neurotrophic factor (PeproTech) + 0.5 mM dbcAMP (Sigma Aldrich). Media was refreshed twice a week for three weeks. After three weeks, neurons were selected for CD184/CD44/CD271 negative population by MACS sorting and plated for experiments. For microglial differentiation iPSCs were

differentiated into hematopoietic progenitor cells (HPCs) using the STEMdiff™ Hematopoietic Kit (05310, Stem cell Technologies). HPCs were either frozen using Bambanker HRM freezing media (BBH01, Bulldog Bio) or further differentiated into MGLs. HPCs were cultured in microglia differentiation medium comprised of DMEM/F12 (11039047, Thermo Fisher Scientific), B27 (17504–044, Thermo Fisher Scientific), N2 (17502–048, Thermo Fisher Scientific), insulin-transferrin-selenite (41400045, Thermo Fisher Scientific), non-essential amino acids (#11140050; Thermo Fisher Scientific), Glutamax (#35050061; Thermo Fisher Scientific), human insulin (I2643-25mg, Sigma) and monothioglycerol (M1753, Sigma) supplemented with 25 ng/ml human M-CSF (PHC9501, Thermo Fisher Scientific), 50 ng/ml TGF-β1 (130-108-969, Miltenyi), and 100 ng/ml IL-34 (200–34, PeproTech). After 24 days in this medium, two additional cytokines, 100 ng/ml CD200 (C311, NovoProtein) and 100 ng/ml CX3CL1 (300–31, PeproTech), were added to the medium described above to mature MGLs. MGLs were cultured in this new medium for an additional week and then harvested for experiments.

For mRNA expression analysis, RNA was extracted using the Trizol (15596018, Thermo Fisher Scientific) and first strand cDNA synthesis was performed using the iScript cDNA Synthesis kit (1708890, Bio-Rad). Quantitative PCR (qPCR) was performed with SYBR Green Master Mix (A46012, Thermo Fisher Scientific). SYK and FCER1G values were normalized to the geometric mean of the housekeeping genes, RPL13 and CYC1. qRT-PCR results were calculated using the  $2^{-DDCT}$  method and presented as fold change from DMSO following the procedure described by Rao and co-workers [50].

Primer sequences:

SYK Primer #4:

Forward 5' GAGAAAGGAGAGCGGATGGG 3'

Reverse 5' GGGCCTGTTTTCCACATCGT 3'

SYK Primer #8

Forward 5' AGGTTTCCATGGGCATGAAGT 3'

Reverse 5' CATGGGTCTGGGCCTTGTA 3'

FCER1G Primer #1

Forward 5' TGGTGTTTACACGGGCCTGA 3'

Reverse 5' CCATGAGGGCTGGAAGAACC 3'

FCER1G Primer #2

Forward 5' CGATCTCCAGCCCAAGATGA 3'

Reverse 5' CCTTTCGCACTTGGATCTTCA 3'

## Bioinformatics

Risk score calculation and biological domain definitions are described in Cary *et al.* [33]. Pre-computed Target Risk Scores (syn25575156, v13), genetic risk scores (syn26844312, v6), and multi-omics risk scores (syn22758536, v9), were downloaded from Synapse. Single cell data (SEAAD\_MTG\_RNAseq\_final-nuclei.2022-08-18.h5ad) were downloaded from the provided Amazon Web Services S3 bucket (s3://sea-ad-single-cell-profiling/MTG/RNAseq/) and processed with a custom script. Briefly, the script groups single cells based on the Supertype label as well as the Cognitive Status of the donor and computes an average expression for each gene as well as the fraction of cells with > 0 counts for that gene. Results were plotted using custom R scripts. All code used to process these data are available ([github.com/caryga/TREATAD\\_target\\_reports](https://github.com/caryga/TREATAD_target_reports)).

## Protein purification

SYK-tSH2 protein was produced using *E. coli* BL21(DE3)-R3-pRARE cells grown in terrific broth. Prior to harvesting, cells were shifted to 18°C for 16 h after IPTG induction. For biotinylation of SYKA-c022 containing the AviTag, biotin (300 μM final) was added to the culture at the same time as IPTG addition. Cells were lysed by sonication in Lysis Buffer containing 50 mM HEPES (pH 7.5), 500 mM NaCl, 10 mM imidazole, 5% glycerol, 1 mM TCEP. SYK-tSH2 protein was bound to equilibrated Ni-IDA resin for 1 h before two batch washes in Lysis Buffer. Beads were subsequently loaded onto a drip column, followed by washing with Lysis Buffer containing 30 mM imidazole, before finally eluting bound protein with Lysis Buffer containing 300 mM imidazole. For TR-FRET assays, the 6xHis tag on SYKA-c020 was left intact. For biophysical assays, the 6xHis tag on SYKA-c020 or SYKA-c022 was cleaved off by the addition of a 1:10 mass ratio of 6xHis-TEV protease while undergoing dialysis (10k MWCO) in Lysis Buffer lacking imidazole for 16 h at 4°C. TEV protease and the cleaved 6xHis tag was subsequently removed with Ni-IDA resin equilibrated in Lysis Buffer. The molecular mass of purified proteins was confirmed by mass spectroscopy.

## Kinetic solubility

Analiza, Inc. analyzed the kinetic solubility of a 5 mM DMSO stock of **44** and a freshly prepared 10 mM stock of **42** dissolved in phosphate buffered saline (PBS) solution at pH 7.4. Following 24 h incubation in a Millipore solubility filter plate, samples were vacuum filtered, and the filtrates collected for analysis. Filtrates were injected into the nitrogen detector for quantification via total chemiluminescent nitrogen determination (CLND). Filtrates were quantified with respect to a calibration curve generated using standards that span the dynamic range of the instrument. The reported solubility value has been corrected for background nitrogen present in the media and DMSO.

## TR-FRET Assay

TR-FRET experiments were performed in 20 μL reactions, using 384-well shallow-well microplates (PerkinElmer). Final reaction components contained 6xHis-SYK-tSH2 (SYKA-c020 tagged) (4 nM), FITC-conjugated FCER1G peptide (8 nM), Tb-conjugated anti-6xHis antibody (53 ng/ml; Cisbio) in assay buffer containing 25 mM HEPES (pH 7.5), 200 mM NaCl, 0.1% BSA and 0.05% Tween-20. After a 2h incubation (at room temperature), TR-FRET signals were measured on a BMG Labtech PHERAstar FSX reader using a Lanthascreen Optics Module. A 200 μs delay was used after excitation with a flash lamp before measurement of fluorescence emission at 490 and 520 nm. TR-FRET ratios of fluorescent intensity at 520 nm to 490 nm were calculated. The half maximal inhibitory concentration (IC50) was determined by fitting a four parametric logistic curve to the data.

## High-throughput TR-FRET Assay

The TR-FRET assay for 6xHis-SYK-tSH2 (SYKA-c020 tagged) and FITC-FCER1G peptide interaction was miniaturized and optimized into a 1536-well format for uHTS (details of the assay miniaturization will be described in a separate publication). The uHTS was performed in black 1536-well plate (3724, Corning costar) with a total volume of 5 μL in each well. 5 μL of the reaction mixture containing optimized concentrations of protein and peptide (6xHis-SYK-tSH2 protein: 2 nM, FITC-p-FCER1G: 6 nM, and anti-His-Tb 1:1000) was dispensed into black 1536-well plates using multiple-drop Combi dispenser (5840320, Thermo). The FITC-p-FCER1G and anti-His-Tb without His-SYK protein was used as background control. 0.1 μL of



library compound dissolved in DMSO was added using pintool integrated with Beckman NX (Beckman Coulter, Brea, CA). The final compound concentration was 20  $\mu\text{M}$  and the final DMSO concentration was 2%. The TR-FRET signals were measured using PHERAstar FSX plate reader (BMG) as described above. A total of 138,214 compounds from two chemical diversity libraries (ChemDiv and Asinex) at Emory Chemical Biology Discovery Center (ECBDC) have been screened.

Screening data were analyzed using Bioassay software from CambridgeSoft (Cambridge, MA). The S/B and Z' in uHTS format were calculated for each screening plate. The effect of compound on the interaction TR-FRET signal was expressed as % of Control and calculated as the following equation:

$$\% \text{ of Control} = (F \text{ compound} - F \text{ Background}) / (F \text{ control} - F \text{ background}) \times 100$$

Where F control and F background are the average TR-FRET signal from highest signal (His-SYK protein and FITC-p-FCER1G) and background without His-SYK protein (lowest signal), respectively. F compound is the TR-FRET signal for His-SYK/FITC-p-FCER1G interaction in the presence of library compound. Compounds that caused % Control < 60 were defined as primary positives.

### Differential Scanning Fluorimetry (DSF)

SYK-tSH2 protein (SYKA-c020 cleaved), lacking the N-terminal 6xHis tag, was diluted in assay buffer (2  $\mu\text{M}$  in 10 mM HEPES, 150 mM NaCl) containing Sypro Orange (1 in 1000 dilution; Thermo Fisher). Compounds, control peptides (1  $\mu\text{M}$ ), or DMSO was added to SYK-tSH2 to 2% of final volume and the mixture was incubated for 30 min on ice. Melting curves were obtained on an Mx3005p qPCR machine (Agilent), ramping up from 25 to 95°C, at 1°C min<sup>-1</sup>. Data were fitted GraphPad Prism to the Boltzmann equation. The  $T_m$  was calculated by determining the maximum value of the first derivative of fluorescence transition.

### GST-PD

The dose response confirmatory GST pulldown with test compounds was performed using the following reagents: Glutathione Sepharose 4B (17075605, Cytiva Sweden AB); WB primary antibodies: GST-Taq (2.6H1) Mouse mAb (2624S, Cell Signaling) 1:1000 dilution in TBST; Monoclonal Anti-FLAG M2-HRP antibody (A8592-1MG, Sigma) 1:1000 dilution in TBST; Fc $\epsilon$ R1 mouse monoclonal antibody (SC-390222, Santa Cruz). WB secondary antibodies: peroxidase-conjugated AffiniPure Goat Anti-Mouse IgG (H+L) (115-035-003, Jackson Immuno Research) 1:5000 dilution in TBST. GST pulldown was performed as described with minor changes [51]. HEK293T (CRL-3216, ATCC) were cultured in Dulbecco's modified Eagle's medium with 4.5 g/L glucose, L-glutamine, and sodium pyruvate (10-013-CV, Corning) supplemented with 10% fetal bovine serum and 1% penicillin/streptomycin solution (30-002-CI, CellGro). Cells were incubated at 37°C in humidified conditions with 5% CO<sub>2</sub>. The HEK293T cells were transfected using 1 mg/mL Polyethylenimine (PEI; 23966, Polysciences) in a ratio of 3  $\mu\text{L}$  to 1  $\mu\text{g}$  DNA. The proteins were expressed for 48 h at 37°C. Cell pellets were re-suspended in the SYK lysis buffer (25 mM HEPES, pH 7.5, 200 mM NaCl, 0.5% Triton X100 (T9284-1L, Sigma-Aldrich), followed by sonication for 10 s (5 s on, 5 s off) at 4°C. Cells were pelleted by 10 min centrifugation at 13,000 rpm at 4°C. The cleared lysates were first pre-incubated with compounds for 30 min and then incubated with glutathione sepharose 4B beads (17075605, Cytiva Sweden AB) at 4°C for 2 h with rotation. After the incubation, beads were washed three times with the SYK lysis buffer, eluted by boiling in sodium dodecyl sulfate-polyacrylamide gel

electrophoresis (SDS–PAGE) loading buffer (1610737, Bio-Rad), and analyzed by western blotting.

### Bio-layer interferometry

Bio-Layer Interferometry (BLI) for compound/protein direct binding was performed using the Octet RED384 system (Sartorius BioAnalytical Instruments) and biotinylated SYK-tSH2 protein (SYKA-c022 cleaved/biotinylated) (as previously described). The biotinylated SYK-tSH2 (50 µg/mL) was loaded onto super streptavidin sensors in 50 µL loading buffer (PBS + 0.02% Tween-20) for 10 min resulting in a 14 nm loading density. The assay was performed as described in [52].

### Compound solubility with nephelometer

Stock compound (10 mM in DMSO) was serially diluted in PBS (21-040-CV, Corning) in 96-well Costar Assay plate (3904, Corning). After incubating compound in PBS for 90 min at room temperature, the Nephelometric turbidity units (NTUs) were measured with NEPHELOstar (BMG LABTECH, Cary, North Carolina). 0.2 s was used for a measure time and PBS only as the background. Each sample was tested in triplicate. Dose-response data was analyzed by GraphPad Prism and the solubility concentration is defined at the concentration that increases the NTUs at the turning point of the curve.

### Covalent labelling and mass spectrometry of proteins

Proteins were diluted to 80 µg/ml in buffer containing 50 mM HEPES (pH 7.5) and 200 mM NaCl before the addition of compounds to test for covalently labelling, giving a final concentration of 2% DMSO in the reaction. After incubation for 1 h at room temperature, the reaction was stopped by the addition of 4 volumes of 0.2% formic acid. Reversed-phase chromatography was performed in-line prior to mass spectrometry using an Agilent 1100 HPLC system (Agilent Technologies inc.–Palo Alto, CA, USA). Protein samples in formic acid were injected (50 µL) on to a 2.1 mm x 12.5 mm *Zorbax* 5µm 300SB-C3 guard column housed in a column oven set at 40 °C. The solvent system used consisted of 0.1% formic acid in ultra-high purity water (Millipore) (solvent A) and 0.1% formic acid in methanol (LC-MS grade, Chromasolve) (solvent B). Chromatography was performed as follows: Initial conditions were 90% A and 10% B and a flow rate of 1.0 ml/min. After 15 s at 10% B, a two-stage linear gradient from 10% B to 80% B was applied, over 45 s and then from 80% B to 95% B over 3 s. Elution then proceeded isocratically at 95% B for 1 min 12 s followed by equilibration at initial conditions for a further 45 s. Protein intact mass was determined using a 1969 MSD-ToF electrospray ionisation orthogonal time-of-flight mass spectrometer (Agilent Technologies Inc.–Palo Alto, CA, USA). The instrument was configured with the standard ESI source and operated in positive ion mode. The ion source was operated with the capillary voltage at 4000 V, nebulizer pressure at 60 psi, drying gas at 350 °C and drying gas flow rate at 12 L/min. The instrument ion optic voltages were as follows: fragmentor 250 V, skimmer 60 V and octopole RF 250 V.

### Purchase of commercial compounds

Reagents were obtained from verified commercial suppliers and used without further characterization or purification. **1** (Compound B in Visperas *et al.* [27], CAS:378201-55-9). **37** (PubChem ID: 24319153) was purchased from Vitas-M Laboratory (Vendor ID: STL228089). **13** (PubChem ID: 24337874) was purchased from Enamine (Vendor ID: Z56176033).

Compounds **2–41** were purchased from ChemDiv, ChemBridge, Vitascreen, LifeChemicals, and Enamine. Other UNC compounds (**42**, **43**, **46–60**) were purchased from ChemSpace.

## Chemistry

**General information.** Temperatures are reported in degree Celsius ( $^{\circ}\text{C}$ ); the solvent was removed via a rotary evaporator under reduced pressure; and thin layer chromatography was used to monitor the progress of reactions that were executed unless otherwise noted. The following abbreviations are used in schemes and/or experimental procedures:  $\mu\text{mol}$  (micromoles), mg (milligrams), equiv (equivalent(s)), and h (hours).  $^1\text{H}$  NMR and/or additional microanalytical data were collected for intermediates and final compounds to confirm their identity and assess their purity.  $^1\text{H}$  spectra were obtained in  $\text{DMSO-}d_6$  and recorded using Varian or Bruker spectrometers. Magnet strength is indicated in the line listing. Peak positions are listed in parts per million (ppm) and calibrated versus the shift of the indicated deuterated solvent; coupling constants ( $J$  values) are reported in hertz (Hz); and multiplicities are included as follows: singlet (s). Purity was determined using high-performance liquid chromatography (HPLC). All final compounds are  $>95\%$  pure by HPLC analysis.

## Synthesis of **44**

*8,8'-disulfanediybis(1,3-dimethyl-3,7-dihydro-1H-purine-2,6-dione)* (**44**). To a flask was added 1,3-dimethyl-8-thioxo-3,7,8,9-tetrahydro-1H-purine-2,6-dione (100 mg, 1 equiv., 471  $\mu\text{mol}$ ) and DMF (2.36 mL) and the reaction refluxed at  $100^{\circ}\text{C}$  for 4 h until a yellow precipitate crashed out. The precipitate was washed with  $\text{H}_2\text{O}$  under vacuum filtration and further dried under vacuum to yield the desired product as a yellow solid, 8'-disulfanediybis(1,3-dimethyl-3,7-dihydro-1H-purine-2,6-dione) (38 mg, 19%).  $^1\text{H}$  NMR (400 MHz,  $\text{DMSO-}d_6$ ):  $\delta$  3.42 (s, 3H), 3.25 (s, 3H). LCMS Calculated for  $\text{C}_{14}\text{H}_{15}\text{N}_8\text{O}_4\text{S}_2$   $[\text{M}+\text{H}]^+$ : 423.06. Found: 423.0. MP:  $>300^{\circ}\text{C}$ .

## Supporting information

**S1 Table. uHTS follow-up structures and associated data.** Chemical structures of the initial hit from uHTS (**39**) and analogues purchased based on this hit compound. TR-FRET data are reported as the  $\text{IC}_{50} \pm$  standard deviation ( $n = 3$ ). DSF data are reported as  $\Delta\text{Tm} \pm$  standard deviation ( $n = 3$ ). <sup>a</sup> TR-FRET data from initial uHTS. NT = Not tested. (PDF)

**S1 Fig. Gel filtration fractions and intact mass deconvolution of purified SYK proteins.** (A) SYKA-c020 His tagged, (B) SYKA-c020 His tag cleaved, and (C) SYKA-c020 His tag cleaved and biotinylated. (TIFF)

**S2 Fig. Second biological replicate of GST-PD data displayed in Fig 4B and dose-response GST-PD for compounds **4** and **32**.** (A) Compounds **4**, **13**, **24**, **32**, and **37**, **4**, were able to inhibit the interaction between SYK-GST and FCER1G-Flag in a pulldown assay at a single concentration (100  $\mu\text{M}$ ). Second biological replicate displayed. (B) Dose-response GST-PD of **4** and **32**. Unmodified gels corresponding with panels (A) and (B) are included in [S7 Fig](#). (TIFF)

**S3 Fig. Secondary biophysical analyses of hit compounds via BLI.** (A) **37**, (B) **13**, (C) **44**, (D) **42** (fresh DMSO stock–monomer compound), (E) **42** (assumed mixture of monomer and

disulfide) BLI data.  
(TIFF)

**S4 Fig. Identification of active disulfide compounds which form in DMSO solutions of compounds 42 and 43.** (A) LCMS analysis of **42** as a fresh solution in MeCN indicates the monomer is present. LCMS Calculated for  $[M+H]^+$   $C_7H_9N_4O_2S$ : 213.04; observed: 213.1  $[M+H]^+$ . (B) LCMS analysis of **42** 10 mM stock solution in MeCN indicates the disulfide dimer is present. LCMS Calculated for  $[M+H]^+$   $C_{14}H_{15}N_8O_4S_2$ : 423.06; observed: 423.0  $[M+H]^+$ . (C) LCMS analysis of **43** as a fresh solution in MeCN indicates the monomer is present. LCMS Calculated for  $[M+H]^+$   $C_{10}H_{15}N_4O_2S$ : 255.08; observed: 255.1  $[M+H]^+$ . (D) LCMS analysis of **43** 10 mM stock solution in MeCN indicates the disulfide dimer is present. LCMS Calculated for  $[M+H]^+$   $C_{20}H_{27}N_8O_4S_2$ : 507.15; observed: 507.1  $[M+H]^+$ .  
(TIFF)

**S5 Fig. Measurements of solubility of compounds 13 and 37 in PBS by nephelometer.**  
(PDF)

**S6 Fig. Mass spectrometry of compound 44 incubated at 30 and 100  $\mu$ M at rt for 1 h with proteins.** (A) SYK, (B) SHIP1, (C) TBXT, (D) MSN.  
(PDF)

**S7 Fig. Original uncropped and unadjusted images underlying blots or gels.** These images correspond with data included in Table 1 as well as blots in Figs 4A–4C, 6H, and S2A, S2B Fig.  
(PDF)

**S8 Fig. Spectral characterization of compound 44.**  $^1H$  NMR and LCMS spectra that confirm identity and purity of compound 44.  
(PDF)

## Acknowledgments

The authors thank Drs. Allan I. Levey, Lara M. Mangravite, Aled Edwards, Frank Longo, Tim M. Willson, and Stephen V. Frye for insightful discussions and suggestions during the development of these resources. The Target Enablement to Accelerate Therapy Development for Alzheimer's Disease (TREAT-AD) Consortium was established by the National Institute on Aging (NIA). Members of Emory-Sage-SGC TREAT-AD Center include: Ishita Ajith<sup>1</sup>, Joel K. Annor-Gyamfi<sup>2</sup>, Jeff Aube<sup>2</sup>, Alison D. Axtman<sup>2</sup>, Frances M. Bashore<sup>2</sup>, Ranjita S. Betarbet<sup>3</sup>, Juan Botas<sup>4</sup>, William J. Bradshaw<sup>1</sup>, Paul E. Brennan<sup>1</sup>, Peter J. Brown<sup>2</sup>, Robert R. Butle<sup>r</sup> 3rd<sup>5</sup>, Jacob L. Capener<sup>2</sup>, Gregory W. Carter<sup>6</sup>, Gregory A. Cary<sup>6</sup>, Catherine Chen<sup>4</sup>, Rachel Commander<sup>3</sup>, Sabrina Daghli<sup>2</sup>, Suzanne Doolen<sup>7</sup>, Yuhong Du<sup>3</sup>, Aled M. Edwards<sup>8,\*</sup>, Michelle E. Etoundi<sup>4</sup>, Kevin J. Frankowski<sup>2</sup>, Stephen V. Frye<sup>2</sup>, Haian Fu<sup>3</sup>, Opher Gileadi<sup>1</sup>, Marta Glavatsikh<sup>2</sup>, Jake Gockley<sup>9</sup>, Katerina Gospodinova<sup>1</sup>, Anna K. Greenwood<sup>9</sup>, Peter A. Greer<sup>10</sup>, Lea T. Grinberg<sup>11</sup>, Shiva Guduru<sup>2</sup>, Levon Halabelian<sup>8</sup>, Crystal Han<sup>5</sup>, Brian Hardy<sup>2</sup>, Laura M. Heath<sup>9</sup>, Stephanie Howell<sup>2</sup>, Andrey A. Ivanov<sup>3</sup>, Suman Jayadev<sup>12</sup>, Vittorio L. Katis<sup>1</sup>, Stephen Keegan<sup>6</sup>, May Khanna<sup>13</sup>, Dmitri Kireev<sup>2</sup>, Carl LaFlamme<sup>14</sup>, Karina Leal<sup>9</sup>, Tom V. Lee<sup>4</sup>, Tina M. Leisner<sup>2</sup>, Allan I. Levey<sup>3,\*</sup>, Qianjin Li<sup>3</sup>, David Li-Kroeger<sup>4</sup>, Zhandong Liu<sup>4</sup>, Benjamin A. Logsdon<sup>9</sup>, Frank M. Longo<sup>5</sup>, Lara M. Mangravite<sup>9</sup>, Peter S. McPherson<sup>14</sup>, Richard M. Nwankama<sup>3</sup>, Felix O. Nwogbo<sup>2</sup>, Carolyn A. Paisie<sup>6</sup>, Arti Parihar<sup>12</sup>, Kenneth H. Pearce<sup>2</sup>, Kun Qian<sup>3</sup>, Min Qui<sup>3</sup>, Stacey J Sukoff Rizzo<sup>7</sup>, Karolina A. Rygiel<sup>1</sup>, Julie Schumacher<sup>5</sup>, David D. Scott<sup>15</sup>, Nicholas T. Seyfried<sup>3</sup>, Joshua M. Shulman<sup>4</sup>, Ben Siciliano<sup>3</sup>, Arunima Sikdar<sup>2</sup>, Nathaniel Smith<sup>4</sup>, Michael Stashko<sup>2</sup>, Judith A. Tello Vega<sup>15</sup>, Dilipkumar Uredi<sup>2</sup>, Dongxue Wang<sup>3</sup>, Jianjun Wang<sup>3</sup>,

Xiaodong Wang<sup>2</sup>, Zhexing Wen<sup>3</sup>, Jesse C. Wiley<sup>9</sup>, Alexander Wilkes<sup>1</sup>, Charles A. Williams<sup>12</sup>, Timothy M. Willson<sup>2</sup>, Aliza Wingo<sup>3</sup>, Thomas S. Wingo<sup>3</sup>, Novak Yang<sup>3</sup>, Jessica E. Young<sup>12</sup>, Miao Yu<sup>6</sup>, Elizabeth L. Zoeller.<sup>3\*</sup> \*Leads: Aled M. Edwards and Allan I. Levey, contact: [aled.edwards@utoronto.ca](mailto:aled.edwards@utoronto.ca) and [alevey@emory.edu](mailto:alevey@emory.edu), respectively.

<sup>1</sup>University of Oxford, Oxford, OX3 7FZ, UK

<sup>2</sup>University of North Carolina at Chapel Hill, Chapel Hill, NC 27599, USA

<sup>3</sup>Emory University School of Medicine, Atlanta, GA 30322, USA

<sup>4</sup>Baylor College of Medicine, Houston, TX 77030, USA

<sup>5</sup>Stanford University School of Medicine, Stanford, CA, 94305, USA

<sup>6</sup>The Jackson Laboratory, Bar Harbor, ME 04609, USA

<sup>7</sup>University of Pittsburgh School of Medicine, Pittsburgh, PA 15219, USA

<sup>8</sup>University of Toronto, Toronto, ON M5G 1L7, Canada

<sup>9</sup>Sage Bionetworks, Seattle, WA, 98121, USA

<sup>10</sup>Queen's University, Kingston, Ontario, ON K7L 3N6, Canada

<sup>11</sup>University of California, San Francisco, San Francisco, CA 94143, USA

<sup>12</sup>University of Washington, Seattle, WA 98109, USA

<sup>13</sup>New York University, New York, NY 10010, NY, USA

<sup>14</sup>McGill University, Montreal, QC H3A 2B4, Canada

<sup>15</sup>University of Arizona, Tucson, AZ 85724, USA

## Author Contributions

**Conceptualization:** Frances M. Bashore, Vittorio L. Katis, Yuhong Du, Opher Gileadi, Paul E. Brennan, Jesse C. Wiley, Gregory A. Cary, Gregory W. Carter, Jessica E. Young, Kenneth H. Pearce, Haian Fu, Alison D. Axtman.

**Data curation:** Frances M. Bashore, Vittorio L. Katis, Yuhong Du, Arunima Sikdar, Dongxue Wang, William J. Bradshaw, Karolina A. Rygiel, Tina M. Leisner, Rod Chalk, Swati Mishra, C. Andrew Williams, Jesse C. Wiley, Jake Gockley, Gregory A. Cary.

**Formal analysis:** Frances M. Bashore, Vittorio L. Katis, Yuhong Du, Arunima Sikdar, William J. Bradshaw, Karolina A. Rygiel, Tina M. Leisner, Rod Chalk, Swati Mishra, C. Andrew Williams, Jesse C. Wiley, Jake Gockley, Gregory A. Cary.

**Funding acquisition:** Opher Gileadi, Paul E. Brennan, Gregory W. Carter, Haian Fu, Alison D. Axtman.

**Investigation:** Frances M. Bashore, Vittorio L. Katis, Yuhong Du, Arunima Sikdar, Dongxue Wang, William J. Bradshaw, Karolina A. Rygiel, Tina M. Leisner, Rod Chalk, Swati Mishra, C. Andrew Williams, Jesse C. Wiley, Jake Gockley, Gregory A. Cary.

**Methodology:** Frances M. Bashore, Vittorio L. Katis, Yuhong Du, Arunima Sikdar, Dongxue Wang, William J. Bradshaw, Karolina A. Rygiel, Tina M. Leisner, Rod Chalk, Swati Mishra, C. Andrew Williams, Jesse C. Wiley, Jake Gockley, Gregory A. Cary.

**Project administration:** Alison D. Axtman.

**Resources:** Frances M. Bashore, Vittorio L. Katis, Yuhong Du, Arunima Sikdar, Dongxue Wang, William J. Bradshaw, Karolina A. Rygiel, Tina M. Leisner, Rod Chalk, Swati Mishra, C. Andrew Williams, Jesse C. Wiley, Jake Gockley, Gregory A. Cary.

**Supervision:** Opher Gileadi, Paul E. Brennan, Jesse C. Wiley, Gregory W. Carter, Jessica E. Young, Kenneth H. Pearce, Haian Fu, Alison D. Axtman.

**Validation:** Frances M. Bashore, Vittorio L. Katis, Yuhong Du, Arunima Sikdar, Dongxue Wang, William J. Bradshaw, Karolina A. Rygiel, Tina M. Leisner, Rod Chalk, Swati Mishra, C. Andrew Williams, Jesse C. Wiley, Jake Gockley, Gregory A. Cary.

**Visualization:** Frances M. Bashore, Vittorio L. Katis, Yuhong Du, Jesse C. Wiley, Gregory A. Cary.

**Writing – original draft:** Frances M. Bashore.

**Writing – review & editing:** Frances M. Bashore, Vittorio L. Katis, Yuhong Du, Arunima Sikdar, Dongxue Wang, William J. Bradshaw, Karolina A. Rygiel, Tina M. Leisner, Rod Chalk, Swati Mishra, C. Andrew Williams, Opher Gileadi, Paul E. Brennan, Jesse C. Wiley, Jake Gockley, Gregory A. Cary, Gregory W. Carter, Jessica E. Young, Kenneth H. Pearce, Haian Fu, Alison D. Axtman.

## References

1. Sada K, Takano T, Yanagi S, Yamamura H. Structure and function of Syk protein-tyrosine kinase. *J Biochem.* 2001; 130(2): 177–86. <https://doi.org/10.1093/oxfordjournals.jbchem.a002970> PMID: 11481033
2. Siraganian RP, de Castro RO, Barbu EA, Zhang J. Mast cell signaling: the role of protein tyrosine kinase Syk, its activation and screening methods for new pathway participants. *FEBS Lett.* 2010; 584(24): 4933–4940. <https://doi.org/10.1016/j.febslet.2010.08.006> PMID: 20696166
3. Brandsma AM, Hogarth PM, Nimmerjahn F, Leusen JHW. Clarifying the Confusion between Cytokine and Fc Receptor “Common Gamma Chain”. *Immunity.* 2016; 45(2): 225–226.
4. Ben Mkaddem S, Benhamou M, Monteiro RC. Understanding Fc Receptor Involvement in Inflammatory Diseases: From Mechanisms to New Therapeutic Tools. *Front Immunol.* 2019; 10: 811. <https://doi.org/10.3389/fimmu.2019.00811> PMID: 31057544
5. Mansueto MS, Reens A, Rakhilina L, Chi A, Pan BS, Miller JR. A reevaluation of the spleen tyrosine kinase (SYK) activation mechanism. *J Biol Chem.* 2019; 294(19): 7658–7668. <https://doi.org/10.1074/jbc.RA119.008045> PMID: 30923129
6. Bradshaw JM. The Src, Syk, and Tec family kinases: distinct types of molecular switches. *Cell Signal.* 2010; 22(8): 1175–1184. <https://doi.org/10.1016/j.cellsig.2010.03.001> PMID: 20206686
7. Kiefer F, Brumell J, Al-Alawi N, Latour S, Cheng A, Veillette A, et al. The Syk Protein Tyrosine Kinase Is Essential for Fcγ Receptor Signaling in Macrophages and Neutrophils. *Mol Cell Biol.* 1998; 18(7): 4209–4220.
8. El-Hillal O, Kurosaki T, Yamamura H, Kinet JP, Scharenberg AM. syk kinase activation by a src kinase-initiated activation loop phosphorylation chain reaction. *Proc Natl Acad Sci.* 1997; 94(5): 1919–1924. <https://doi.org/10.1073/pnas.94.5.1919> PMID: 9050880
9. Burger JA, Wiestner A. Targeting B cell receptor signalling in cancer: preclinical and clinical advances. *Nat Rev Cancer.* 2018; 18(3): 148–167. <https://doi.org/10.1038/nrc.2017.121> PMID: 29348577
10. Wang S, Sudan R, Peng V, Zhou Y, Du S, Yuede CM, et al. TREM2 drives microglia response to amyloid-β via SYK-dependent and -independent pathways. *Cell.* 2022; 185(22): 4153–4169.e19.
11. Varnum MM, Clayton KA, Yoshii-Kitahara A, Yonemoto G, Koro L, Ikezu S, et al. A split-luciferase complementation, real-time reporting assay enables monitoring of the disease-associated transmembrane protein TREM2 in live cells. *J Biol Chem.* 2017; 292(25): 10651–10663. <https://doi.org/10.1074/jbc.M116.759159> PMID: 28490631
12. Mócsai A, Ruland J, Tybulewicz VLJ. The SYK tyrosine kinase: a crucial player in diverse biological functions. *Nat Rev Immunol.* 2010; 10(6): 387–402. <https://doi.org/10.1038/nri2765> PMID: 20467426
13. Buffard M, Naldi A, Freiss G, Deckert M, Radulescu O, Coopman PJ, et al. Comparison of SYK Signaling Networks Reveals the Potential Molecular Determinants of Its Tumor-Promoting and Suppressing Functions. *Biomolecules.* 2021; 11(2): 308. <https://doi.org/10.3390/biom11020308> PMID: 33670716
14. Dasari TK, Geiger R, Karki R, Banoth B, Sharma BR, Gurung P, et al. The nonreceptor tyrosine kinase SYK drives caspase-8/NLRP3 inflammasome-mediated autoinflammatory osteomyelitis. *J Biol Chem.* 2020; 295(11): 3394–3400. <https://doi.org/10.1074/jbc.RA119.010623> PMID: 31719149
15. Schweig JE, Yao H, Coppola K, Jin C, Crawford F, Mullan M, et al. Spleen tyrosine kinase (SYK) blocks autophagic Tau degradation in vitro and in vivo. *J Biol Chem.* 2019; 294(36): 13378–13395. <https://doi.org/10.1074/jbc.RA119.008033> PMID: 31324720

16. Ennerfelt H, Frost EL, Shapiro DA, Holliday C, Zengeler KE, Voithofer G, et al. SYK coordinates neuroprotective microglial responses in neurodegenerative disease. *Cell*. 2022; 185(22): 4135–4152.e22. <https://doi.org/10.1016/j.cell.2022.09.030> PMID: 36257314
17. Chu E, Mychasiuk R, Hibbs ML, Semple BD. Dysregulated phosphoinositide 3-kinase signaling in microglia: shaping chronic neuroinflammation. *J Neuroinflammation*. 2021; 18(1): 276. <https://doi.org/10.1186/s12974-021-02325-6> PMID: 34838047
18. Currie KS, Kropf JE, Lee T, Blomgren P, Xu J, Zhao Z, et al. Discovery of GS-9973, a Selective and Orally Efficacious Inhibitor of Spleen Tyrosine Kinase. *J Med Chem*. 2014; 57(9): 3856–3573. <https://doi.org/10.1021/jm500228a> PMID: 24779514
19. Lam B, Arikawa Y, Cramlett J, Dong Q, De Jong R, Feher V, et al. Discovery of TAK-659 an orally available investigational inhibitor of Spleen Tyrosine Kinase (SYK). *Bioorg Med Chem Lett*. 2016; 26(24): 5947–5950. <https://doi.org/10.1016/j.bmcl.2016.10.087> PMID: 27839918
20. Yamamoto N, Takeshita K, Shichijo M, Kokubo T, Sato M, Nakashima K, et al. The Orally Available Spleen Tyrosine Kinase Inhibitor 2-[7-(3,4-Dimethoxyphenyl)-imidazo[1,2-c]pyrimidin-5-ylamino]nicotinamide Dihydrochloride (BAY 61–3606) Blocks Antigen-Induced Airway Inflammation in Rodents. *J Pharmacol Exp Ther*. 2003; 306(3): 1174–1181. <https://doi.org/10.1124/jpet.103.052316> PMID: 12766258
21. Coffey G, Deguzman F, Inagaki M, Pak Y, Delaney SM, Ives D, et al. Specific Inhibition of Spleen Tyrosine Kinase Suppresses Leukocyte Immune Function and Inflammation in Animal Models of Rheumatoid Arthritis. *J Pharmacol Exp Ther*. 2012; 340(2): 350–359. <https://doi.org/10.1124/jpet.111.188441> PMID: 22040680
22. Braselmann S, Taylor V, Zhao H, Wang S, Sylvain C, Baluom M, et al. R406, an Orally Available Spleen Tyrosine Kinase Inhibitor Blocks Fc Receptor Signaling and Reduces Immune Complex-Mediated Inflammation. *J Pharmacol Exp Ther*. 2006; 319(3): 998–1008. <https://doi.org/10.1124/jpet.106.109058> PMID: 16946104
23. Rolf MG, Curwen JO, Veldman-Jones M, Eberlein C, Wang J, Harmer A, et al. In vitro pharmacological profiling of R406 identifies molecular targets underlying the clinical effects of fostamatinib. *Pharmacol Res Perspect*. 2015; 3(5): e00175. <https://doi.org/10.1002/prp2.175> PMID: 26516587
24. Cooper N, Ghanima W, Hill QA, Nicolson PL, Markovtsov V, Kessler C. Recent advances in understanding spleen tyrosine kinase (SYK) in human biology and disease, with a focus on fostamatinib. *Platelets*. 2023; 34(1): 1–13. <https://doi.org/10.1080/09537104.2022.2131751> PMID: 36331249
25. Liu D, Mamorska-Dyga A. Syk inhibitors in clinical development for hematological malignancies. *J Hematol Oncol*. 2017; 10(1): 145. <https://doi.org/10.1186/s13045-017-0512-1> PMID: 28754125
26. Schweig JE, Yao H, Coppola K, Jin C, Crawford F, Mullan M, et al. Spleen tyrosine kinase (SYK) blocks autophagic Tau degradation in vitro and in vivo. *J Biol Chem*. 2019; 294(36): 13378–13395. <https://doi.org/10.1074/jbc.RA119.008033> PMID: 31324720
27. Patrick Jonathan, Timothy Neel, Diane, Tao A, et al. Modification by covalent reaction or oxidation of cysteine residues in the tandem-SH2 domains of ZAP-70 and Syk can block phosphopeptide binding. *Biochem J*. 2015; 465(1): 149–161. <https://doi.org/10.1042/BJ20140793> PMID: 25287889
28. Schweig JE, Yao H, Beaulieu-Abdelahad D, Ait-Ghezala G, Mouzon B, Crawford F, et al. Alzheimer's disease pathological lesions activate the spleen tyrosine kinase. *Acta Neuropathol Commun*. 2017; 5(1): 69. <https://doi.org/10.1186/s40478-017-0472-2> PMID: 28877763
29. Birkle TJY, Brown GC. Syk inhibitors protect against microglia-mediated neuronal loss in culture. *Front Aging Neurosci*. 2023; 15: 1120952. <https://doi.org/10.3389/fnagi.2023.1120952> PMID: 37009452
30. Cao S, Standaert DG, Harms AS. The gamma chain subunit of Fc receptors is required for alpha-synuclein-induced pro-inflammatory signaling in microglia. *J Neuroinflammation*. 2012; 9: 259. <https://doi.org/10.1186/1742-2094-9-259> PMID: 23186369
31. Komine-Kobayashi M, Chou N, Mochizuki H, Nakao A, Mizuno Y, Urabe T. Dual role of Fc gamma receptor in transient focal cerebral ischemia in mice. *Stroke*. 2004; 35(4): 958–963. <https://doi.org/10.1161/01.STR.0000120321.30916.8E> PMID: 14988576
32. Sierksma A, Lu A, Mancuso R, Fattorelli N, Thrupp N, Salta E, et al. Novel Alzheimer risk genes determine the microglia response to amyloid-β but not to TAU pathology. *EMBO Mol Med*. 2020; 12(3): e10606.
33. Cary G, Wiley J, Gockley J, Keegan S, Heath L, Butler R, et al. Genetic and Multi-omic Risk Assessment of Alzheimer's Disease Implicates Core Associated Biological Domains. *MedRxiv*. 2022; 12.15.22283478.
34. Gabitto MI, Travaglini KJ, Rachleff VM, Kaplan ES, Long B, Ariza J, et al. Integrated multimodal cell atlas of Alzheimer's disease. *BioRxiv*. 2023; 05.08.539485. <https://doi.org/10.21203/rs.3.rs-2921860/v1> PMID: 37292694

35. Doens D, Fernández PL. Microglia receptors and their implications in the response to amyloid  $\beta$  for Alzheimer's disease pathogenesis. *J Neuroinflammation*. 2014; 11(1): 48.
36. Katis V, Bradshaw W, Betarbet R, Fu H, Du Y, Qian K, et al. MSN (Moesin); A Target Enabling Package. Zenodo. 2020; 4429232.
37. Dahlin JL, Walters MA. How to Triage PAINS-Full Research. *Assay Drug Dev Technol*. 2016; 14(3): 168–174. <https://doi.org/10.1089/adt.2015.674> PMID: 26496388
38. Karatas H, Akbarzadeh M, Adihou H, Hahne G, Pobbati AV, Yihui Ng E, et al. Discovery of Covalent Inhibitors Targeting the Transcriptional Enhanced Associate Domain Central Pocket. *J Med Chem*. 2020; 63(20): 11972–11989. <https://doi.org/10.1021/acs.jmedchem.0c01275> PMID: 32907324
39. Chang L, Lee S-Y, Leonczak P, Rozenski J, De Jonghe S, Hanck T, et al. Imidazopyridine- and Purine-Thioacetamide Derivatives: Potent Inhibitors of Nucleotide Pyrophosphatase/Phosphodiesterase 1 (NPP1). *J Med Chem*. 2014; 57(23): 10080–10100. <https://doi.org/10.1021/jm501434y> PMID: 25372276
40. Ren S, Luo N, Liu K, Liu J-B. Synthesis of unsymmetrical disulfides via the cross-dehydrogenation of thiols. *J Chem Res*. 2021; 45(5–6): 365–373.
41. Tam JP, Wu CR, Liu W, Zhang JW. Disulfide bond formation in peptides by dimethyl sulfoxide. Scope and applications. *J Am Chem Soc*. 1991; 113(17): 6657–6662.
42. Settimo AD, Marini AM, Primofiore G, Settimo FD, Bertini D. Synthesis of purinobenzothiazine and pyridothiazinopurine derivatives. Two new heterocyclic ring systems. *J Heterocycl Chem*. 1998; 35(1): 57–60.
43. Morimoto J, Miyamoto K, Ichikawa Y, Uchiyama M, Makishima M, Hashimoto Y, et al. Improvement in aqueous solubility of achiral symmetric cyclofenil by modification to a chiral asymmetric analog. *Sci Rep*. 2021; 11(1): 12697. <https://doi.org/10.1038/s41598-021-92028-y> PMID: 34135380
44. Withnall M, Chen H, Tetko IV. Matched Molecular Pair Analysis on Large Melting Point Datasets: A Big Data Perspective. *ChemMedChem*. 2018; 13(6): 599–606. <https://doi.org/10.1002/cmhc.201700303> PMID: 28650584
45. Hisham M, Youssif BGM, Osman EEA, Hayallah AM, Abdel-Aziz M. Synthesis and biological evaluation of novel xanthine derivatives as potential apoptotic antitumor agents. *Eur J Med Chem*. 2019; 176: 117–128. <https://doi.org/10.1016/j.ejmech.2019.05.015> PMID: 31108261
46. Gabison L, Chiadmi M, El Hajji M, Castro B, Colloc'h N, Prangé T. Near-atomic resolution structures of urate oxidase complexed with its substrate and analogues: the protonation state of the ligand. *Acta Crystallogr D*. 2010; 66(Pt 6): 714–724. <https://doi.org/10.1107/S090744491001142X> PMID: 20516624
47. Ivanov AA, Gonzalez-Pecchi V, Khuri LF, Niu Q, Wang Y, Xu Y, et al. OncoPPI-informed discovery of mitogen-activated protein kinase kinase 3 as a novel binding partner of c-Myc. *Oncogene*. 2017; 36(42): 5852–5860. <https://doi.org/10.1038/onc.2017.180> PMID: 28628118
48. Mishra S, Kinoshita C, Axtman AD, Young JE. Evaluation of a Selective Chemical Probe Validates That CK2 Mediates Neuroinflammation in a Human Induced Pluripotent Stem Cell-Derived Microglial Model. *Front Mol Neurosci*. 2022; 15: 824956. <https://doi.org/10.3389/fnmol.2022.824956> PMID: 35774866
49. Mishra S, Knupp A, Szabo MP, Williams CA, Kinoshita C, Hailey DW, et al. The Alzheimer's gene SORL1 is a regulator of endosomal traffic and recycling in human neurons. *Cell Mol Life Sci*. 2022; 79(3): 162. <https://doi.org/10.1007/s00018-022-04182-9> PMID: 35226190
50. Rao X, Huang X, Zhou Z, Lin X. An improvement of the 2<sup>-ΔΔCT</sup> method for quantitative real-time polymerase chain reaction data analysis. *Biostat Bioinforma Biomath*. 2013; 3(3): 71–85.
51. Yang X, Fan D, Troha AH, Ahn HM, Qian K, Liang B, et al. Discovery of the first chemical tools to regulate MKK3-mediated MYC activation in cancer. *Bioorg Med Chem*. 2021; 45: 116324. <https://doi.org/10.1016/j.bmc.2021.116324> PMID: 34333394
52. Kim YS, Chung H-S, Noh SG, Lee B, Chung HY, Choi J-G. Geraniin Inhibits the Entry of SARS-CoV-2 by Blocking the Interaction between Spike Protein RBD and Human ACE2 Receptor. *Int J Mol Sci*. 2021; 22(16): 8604. <https://doi.org/10.3390/ijms22168604> PMID: 34445310